

Green hydrogen production and liquefaction using offshore wind power, liquid air, and LNG cold energy

Xiaoyuan Chen^a, Jinxin Yue^a, Lin Fu^{b,*}, Mingshun Zhang^a, Miangang Tang^a, Juan Feng^a, Boyang Shen^{c,d,**}

^a School of Engineering, Sichuan Normal University, Chengdu, China

^b Institute of Rail Transit, Tongji University, Shanghai, China

^c Maglev Transportation Engineering R&D Center, Tongji University, Shanghai, China

^d Clare Hall, University of Cambridge, Cambridge, United Kingdom

ARTICLE INFO

Handling Editor: Jin-Kuk Kim

Keywords:

Liquefied natural gas (LNG) cold energy

Off-shore wind energy

Liquid air energy storage (LAES)

Liquid hydrogen production

Techno-economic analysis

ABSTRACT

Coastal regions have abundant off-shore wind energy resources, and surrounding areas have large-scale liquefied natural gas (LNG) receiving stations. From the engineering perspectives, there are limitations in unstable off-shore wind energy and fluctuating LNG loads. This article offers a new energy scheme to combine these 2 energy units, which uses surplus wind energy to produce hydrogen, and use LNG cold energy to liquefy and store hydrogen. In addition, in order to improve the efficiency of utilizing LNG cold energy, and reduce electricity consumption for liquid hydrogen (LH₂) production at coastal regions, this article introduces the liquid air energy storage (LAES) technology as the intermediate stage, which can stably store the cold energy from LNG gasification. A new scheme for LNG-LAES-LH₂ hybrid LH₂ production is built. The case study is based on a real LNG receiving station at Hainan province, China, and this article presents the design of hydrogen production/liquefaction process, and carries out the optimizations at key nodes, and proves the feasibility using specific energy consumption and exergy analysis. In a 100 MW system, the liquid air storage round-trip efficiency is 71.0% and the specific energy consumption is 0.189 kWh/kg, and the liquid hydrogen specific energy consumption is 7.87 kWh/kg and the exergy efficiency is 46.44%. Meanwhile, the corresponding techno-economic model is built, and for a LNG-LAES-LH₂ system with LH₂ daily production 140.4 tons, the shortest dynamic payback period is 9.56 years. Overall, this novel hybrid energy scheme can produce green hydrogen using a more efficient and economical method, and also can make full use of surplus off-shore wind energy and coastal LNG cold energy.

1. Introduction

As a clean fossil energy, natural gas has advantages of high combustion efficiency, less greenhouse gas emissions, and convenient transportation (Khan, 2018). The liquefied natural gas (LNG), generally has a temperature of 111 K (Kochunni and Chowdhury, 2020), and the volume of LNG with the same mass is only 1/625 of gaseous natural gas (Chen et al., 2021), which has much higher energy density and lower transportation cost during the process of trans-ocean and long-distance transportation (Peng et al., 2021).

In China, about 63.44 million tons of LNG were imported in 2022 (General Administration of Customs, People's Republic of China, 2023),

mainly stored in LNG terminals in coastal areas. Most LNG needs to be vaporized through pipelines to users. During the re-gasification process, the cold energy released from per unit mass of LNG is about 830 kJ/kg (Li et al., 2021). In general, LNG cold energy can be used for power generation (Ghorbani et al., 2023), dry ice production (Sung and Kim, 2017), desalination of sea water (Ghasemi et al., 2018), food processing (Cerceanu et al., 2014), etc.

Sun et al. studied three different organic Rankine cycle configurations using LNG cold energy and 8 different potential fluids to increase the exergy efficiency of the system (up to 17.36%) (Sun et al., 2018). Xue et al. proposed a two-stage organic Rankine cycle where exergy efficiency reached 31.02% by using low-grade heat from smoke exhaust and low temperature energy of LNG (Xue et al., 2015). Xia et al. studied and

* Corresponding author. Institute of Rail Transit, Tongji University, Shanghai, China.

** Corresponding author. Maglev Transportation Engineering R&D Center, Tongji University, Shanghai, China

E-mail addresses: lin.fu.2017@outlook.com (L. Fu), bs506@cam.ac.uk (B. Shen).

<https://doi.org/10.1016/j.jclepro.2023.138653>

Received 11 July 2023; Received in revised form 20 August 2023; Accepted 2 September 2023

Available online 4 September 2023

0959-6526/© 2023 The Authors. Published by Elsevier Ltd. This is an open access article under the CC BY license (<http://creativecommons.org/licenses/by/4.0/>).

Nomenclature			
ACS	Air Compression System	LAP	Low-temperature Air Pump
ALP	Air Liquefaction Process	LAT	Liquid Air Tank
ALS	Air Liquefaction System	LH ₂	Liquid Hydrogen
ARS	Air Re-gasification System	LHT	Liquid Hydrogen Tank
EXE	Exergy Efficiency	LNG	Liquefied Natural Gas
GH ₂	Gaseous Hydrogen	NG	Natural Gas
GHT	Gaseous Hydrogen Tank	NPV	Net Present Value
HCS	Hydrogen Compression System	PE	Peak Electricity
HLP	Hydrogen Liquefaction Process	PEMEC	Proton Exchange Membrane Electrolysis Cell
HLS	Hydrogen Liquefaction System	RTE	Round-trip Efficiency
HPS	Hydrogen Pre-cooling System	SEC	Specific Energy Consumption
LA	Liquid Air	TCI	Total Capital Investment
LAES	Liquid Air Energy Storage	VE	Valley Electricity
		WS	Whole System

optimized the solar trans-critical CO₂ power cycle that used LNG cold energy to recover reverse osmosis (RO) desalination process (Xia et al., 2014), and the exergy efficiency of RO desalination process was 4.9%. Zhang et al. designed a stepped cold energy system, including air separation, dry ice making, horizontal two-stage Rankine cycle power generation, seawater desalination, Marine refrigeration, air conditioning and ice making (Zhang et al., 2019), and the exergy efficiency of the optimized system reached 29.57%. However, in these conventional cold energy systems, high-grade cold energy is normally used in high-temperature scenarios, so their exergy efficiencies are relatively low due to the temperature gradient.

In addition to LNG terminals, coastal areas are also rich in clean energy, such as wind, tidal and wave energy. Taking offshore wind power as an example, in 2022, China's installed capacity of offshore wind power has reached 30.89 GW (National Energy Administration, 2023). Due to the instability and volatility of wind power, if surplus wind power is not properly utilized, it will lead to wind curtailment, where a large amount of clean energy can be wasted (Yu et al., 2022). If the surplus wind power is used for electrolytic hydrogen production, the surplus wind power can be converted into stable hydrogen for energy storage (Chen et al., 2023). In order to improve the energy storage density of hydrogen, high-pressure gas tanks are usually used. If using a 700 bar pressure, the hydrogen energy storage density can reach 5.6 MJ/L. However, if the operation pressure of hydrogen storage is large, there could be some risks (e.g., leakage). In order to further improve the energy storage density and reduce the storage pressure, low-temperature liquid hydrogen storage technology scheme can be used, and its energy storage density can reach 10.1 MJ/L, which can be stored in the atmospheric pressure environment (Ratnakar et al., 2021). However, the hydrogen liquefaction process requires a large amount of electricity consumption (12–15 kWh/kg), and it is urgent to optimize the whole process, and improve the energy efficiency of the entire system (Riaz et al., 2022).

At present, one of the solutions is to introduce a mixed refrigerant configured with a variety of substance ratios, combined with some improved pre-cooling cycle methods, which can improve the system efficiency to a certain extent and reduce the specific energy consumption of liquid hydrogen preparation. For instances, the Linde-Hampson cycle, Joule-Brayton refrigeration cycle and water-ammonia absorption refrigeration cycle have been used. The specific energy consumption of liquid hydrogen preparation was reduced to 7.69 kWh/kg (Asadnia and Mehrpooya, 2017), 9.703kWh/kg (Bi and Ju, 2022), 7.405 kWh/kg (Jouybari et al., 2022), and accordingly, their exergy efficiencies were 39.5%, 39.1%, 23.59%.

However, increasing the mixed refrigerant will increase the system investment cost, as well as daily operation and maintenance costs (Yin and Ju, 2020). In addition, exergy loss will surely occur after going

through compressors and heat exchanger equipments, and too much pre-cooling cycle will use more equipments, leading to more exergy loss. Generally, the exergy efficiency of pre-cooling hydrogen is generally lower than 40%.

In order to reduce the complexity of precooling cycle, decrease the specific energy consumption of liquid hydrogen preparation, and increase the exergy efficiency, some scholars have proposed to use low-temperature liquid medium for precooling hydrogen. The LNG cold energy was introduced to pre-cool hydrogen, and the specific energy consumption was reduced to 6.60 kWh/kg (Bian et al., 2021), 7.64 kWh/kg (Riaz et al., 2021a,b), 8.85 kWh/kg (Faramarzi et al., 2021), and their exergy efficiency rose to 47.0%, 42.25%, 47%. For those systems introduced lower temperature liquid nitrogen or air liquefied cold energy to precool hydrogen, the specific energy consumption further reduced to 7.041 kWh/kg (Bi et al., 2022), 5.955 kWh/kg (Taghavi et al., 2021), 7.948 kWh/kg (Bi and Ju, 2022) and 7.25 kWh/kg (Yang et al., 2023), and accordingly, their efficiencies of the system increased to 54.13%, 52.9%, 57.17% and 53.2%.

Existing literatures present that if the cold energy of low temperature medium is used, the exergy efficiency of the system can be improved effectively. If liquefied natural gas is used, the exergy efficiency can be 40%–50%. If liquid air and liquid nitrogen are both used, the exergy efficiency can be further increased to 50%–60%. However, the high cost of liquid nitrogen and liquid air, e.g., \$7.62/kg, is not practical from an economic point of view (Ansarinassab et al., 2023; Xie et al., 2019). Meanwhile, most previous studies directly used liquid nitrogen and liquid air as the energy input of the system, while the exergy loss caused by the production and preparation of liquid air or liquid nitrogen have not been systematically considered (Bi et al., 2022; Bi et al., 2022).

According to literature review and practical engineering investigation, the LNG gasification capacity of LNG receiving stations in coastal areas changes with the change of natural gas load, and the cold energy generated by gasification also changes and fluctuates. Meanwhile, the hydrogen production capacity of offshore wind power also fluctuates with the change of real-time wind speed and grid-connected capacity. Some literatures have studied the use of LNG cold energy to assist liquid hydrogen (LH₂) liquefaction process, which can improve the energy efficiency of the whole system to a certain extent.

Using electrolytic hydrogen production and then using LNG cold energy to liquefy hydrogen has 2 problems:

- (1) The process to balance the real-time fluctuation of LNG gasification cold energy output and the cold energy power demand when producing liquid hydrogen using offshore wind power, can cause the imbalance between cold energy supply and demand, as well as low energy efficiency.

- (2) If all the hydrogen is produced by valley electricity, the system operating cost can be reduced, but the capacity of electrolytic cells needs to be large and thus the initial investment will be high. If a part of the hydrogen is produced by peak electricity, the capacity of electrolytic cells can be smaller and the initial investment will be reduced, but the system operating cost will be higher.

In order to improve the utilization rate of vaporizing cold energy from LNG receiving stations in coastal areas, and reduce the energy consumption of LH₂ produced by offshore wind power, this paper introduces liquid air energy storage (LAES) as an intermediate energy storage link, converts the unstable cold energy during the LNG gasification process into stable cryogenic liquid storage, and build the LNG-LAES-LH₂ hybrid liquid hydrogen scheme. The economic analysis is conducted based on 3 modes of electrolytic hydrogen production, and then the optimal capacity of electrolytic cells is selected to realize the best economic benefits.

Taking an LNG receiving station in Yangpu Economic Development Zone in Danzhou City, Hainan Province, China as a research case, the advantages of the new system have been verified from the perspectives of specific energy consumption and exergy efficiency through the systematic LNG process design, along with the optimization of key parameters. At the same time, this paper also completed the technology-economic modeling evaluation and economic benefit prediction, which can provide a technical solution with high energy efficiency and good economic benefit for the development of large-scale offshore wind power hydrogen production, and coastal LNG integrated system in the future. The technical advantages and main contributions of this novel technology are as follows:

- (1) Liquid air energy storage can properly convert the unstable cold energy in the LNG gasification process into stable cryogenic liquid storage, avoiding the waste of cold energy in LNG gasification.
- (2) Liquid air can provide stable cold energy for pre-cooling in the hydrogen liquefaction process. Liquid air can also generate electricity to supply hydrogen liquefaction equipment by the direct expansion power. The two processes above can greatly reduce the specific energy consumption of hydrogen liquefaction process.
- (3) LNG cold energy is used to pre-cool air, and liquid air cold energy is used to pre-cool hydrogen. As the temperature difference between the cold source and the pre-cooled material becomes minor, the exergy loss is relatively small.
- (4) The use of the cold energy of LNG can reduce the power consumption of the air and hydrogen liquefaction processes, and meanwhile, it can reduce the complexity of the system. Fewer liquefaction process devices can reduce exergy loss and also bring economic benefits.

2. Novel scheme: offshore wind power for hydrogen production and LNG cold energy for hydrogen liquefaction

The LNG receiving station in the Yangpu Economic Development Zone, Danzhou City, Hainan Province, China, receives about 3 million tons of LNG per year (National Energy Administration, 2012). Due to the instability of the gas load, the cold energy of LNG is difficult to be directly recycled (The People's Government of Hainan Province, 2015), and it is urgent for an energy storage device to utilize the cold energy properly.

During the "14th Five-Year Plan" period, the scale of offshore wind power projects in Hainan Province will be 12.3 GW, which is expected to be completed by 2025 (Central Government of the People's Republic of China, 2022). Because of the instability of wind power, it is difficult to get a reasonable absorption, and electrolytic hydrogen production is one

of the effective ways to absorb surplus wind power. Due to the low energy density of hydrogen and the risks of high-pressure transportation, Liquid hydrogen can increase the energy storage density, but also reduce the risk of the transportation. However, the huge energy consumption from the liquefaction process has been restricting the development of liquid hydrogen.

Based on the study (National Energy Communications Newsrooms, 2022), the locations of LNG receiving stations and some offshore wind power are shown in Fig. 1. 4.2 GW offshore wind power will be built near Danzhou City and Lingao City. The LNG receiving station is located in Yangpu Economic Development Zone of Danzhou City, and the offshore wind power and LNG receiving station is very close. Therefore, this paper proposes to use surplus wind power to produce hydrogen, and use LNG cold energy and surplus wind power to liquefy gaseous hydrogen. The entire configuration is shown in Fig. 2.

- (1) LNG cold energy is used to pre-cool the liquid air, and then the surplus electricity from offshore wind power is used to liquefy the air, and tanks are used to store liquid air.
- (2) Surplus wind power from sea is used to produce hydrogen by electrolysis, and tanks are used to store hydrogen.
- (3) In the period of low electricity consumption, the liquid air cold energy is used to pre-cool hydrogen, and the high-pressure air after heat exchange pass through the expansion machine to generate electricity, and the generated electricity is used for the hydrogen liquefaction.

3. The proposed LNG-LAES-LHES system

3.1. System description

Fig. 3 shows the flow chart of the system, which is composed of 6 subsystems, namely, air compression system, air liquefaction system, air re-gasification system, hydrogen precooling system, hydrogen compression system and hydrogen liquefaction system. The specific liquefaction process is as follows:

- (1) The air compression system is heavy (ACS). The air at room temperature atmospheric pressure is fed into the node A1, and the air is pressurized by the two-stage air compressor (AC1, AC2). The air compression process results in the increase of temperature. The air is cooled by condenser 1 and condenser 2, and high-pressure, room temperature air is obtained at node A5.
- (2) In the air liquefaction system (ALS), the high-pressure room temperature air (node A5) is pre-cooled in the cold box by the cold energy of LNG gasification, and the low temperature air has not been completely liquefied in the previous liquefaction process. After the pre-cooling, the temperature of the high-pressure air is reduced to 112.45 K, and finally goes through the pressure reduction control valve TV-1. The high-pressure air reduces its pressure to normal, and its temperature also further reduces. Then, the air is liquefied, and stored in the liquid air tank. A part of the cold air that has not been completely liquefied will be further fed back to a new round of air liquefaction, in order to make full use of cold energy and improve the system energy efficiency.
- (3) The liquid air re-gasification system (ARS) is set to mainly operate at night. After the liquid air is pressurized by a low-temperature air pump (LAP), it is further heated by a heat exchanger (HE-1) with the refrigerant in the hydrogen precooling system (HPS), and the heated air is used to generate electricity by a two-stage air turbine (AT1, AT2). As the expanded air temperature is reduced, a two-stage heater (heater1, heater2) is used to further heat the lower temperature air, which can increase the power generation capacity of the air turbine.

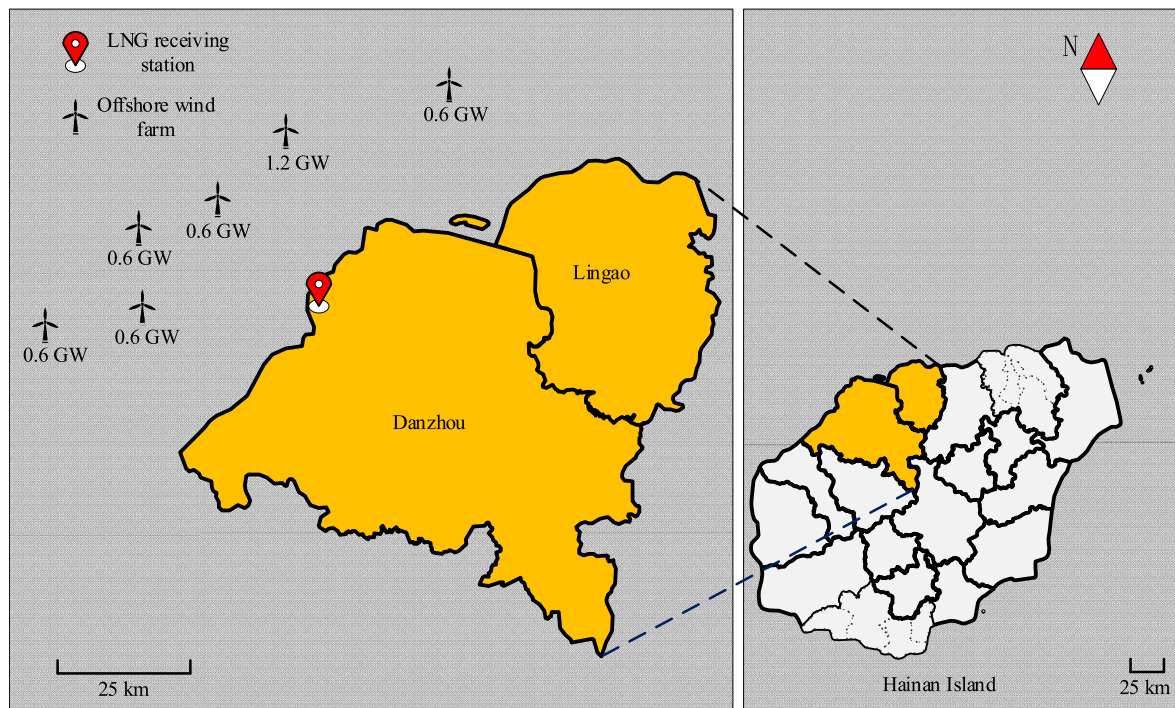


Fig. 1. Geographical locations of offshore wind power and LNG receiving stations.

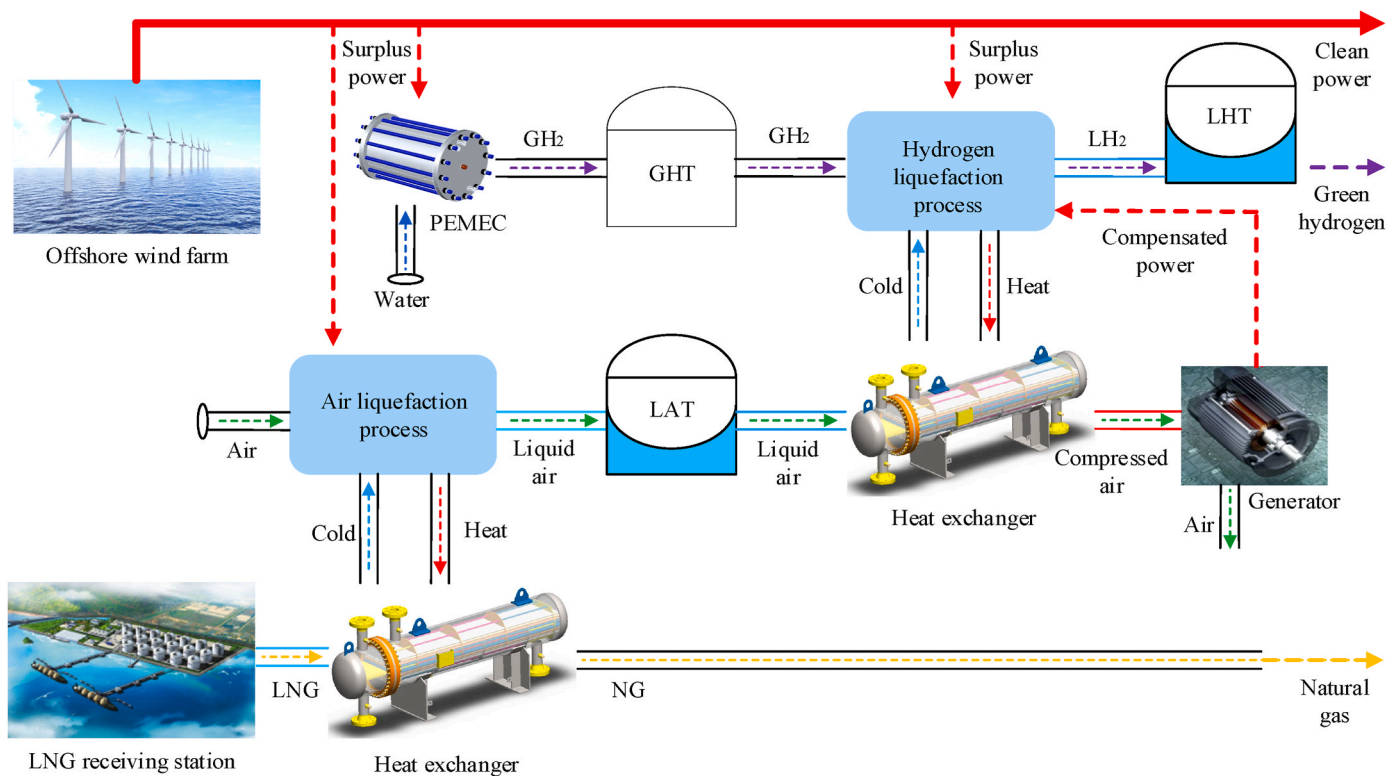


Fig. 2. Novel configuration: using surplus offshore wind power to produce hydrogen, and meanwhile using LNG cold energy to liquify hydrogen.

(4) In the hydrogen pre-cooling system (HPS), the three-stage hydrogen compressor (HC1, HC2, HC3) is used to pressurize the refrigerant at room temperature, and the refrigerant temperature is reduced by cooler 3 and cooler 4, which can reduce the power consumption of hydrogen compressor 2 and hydrogen compressor 3. The cooler 5 can cool the high-temperature

refrigerant to room temperature, and then exchange heat with the liquid air through the heat exchanger HE-1, and the temperature is reduced to 86.95 K. Hydrogen turbine (HT) can be used to generate electricity. This electrical power together with the output of AT1 and AT2 compensate the power demand of hydrogen liquefaction, and thus reduce the total power

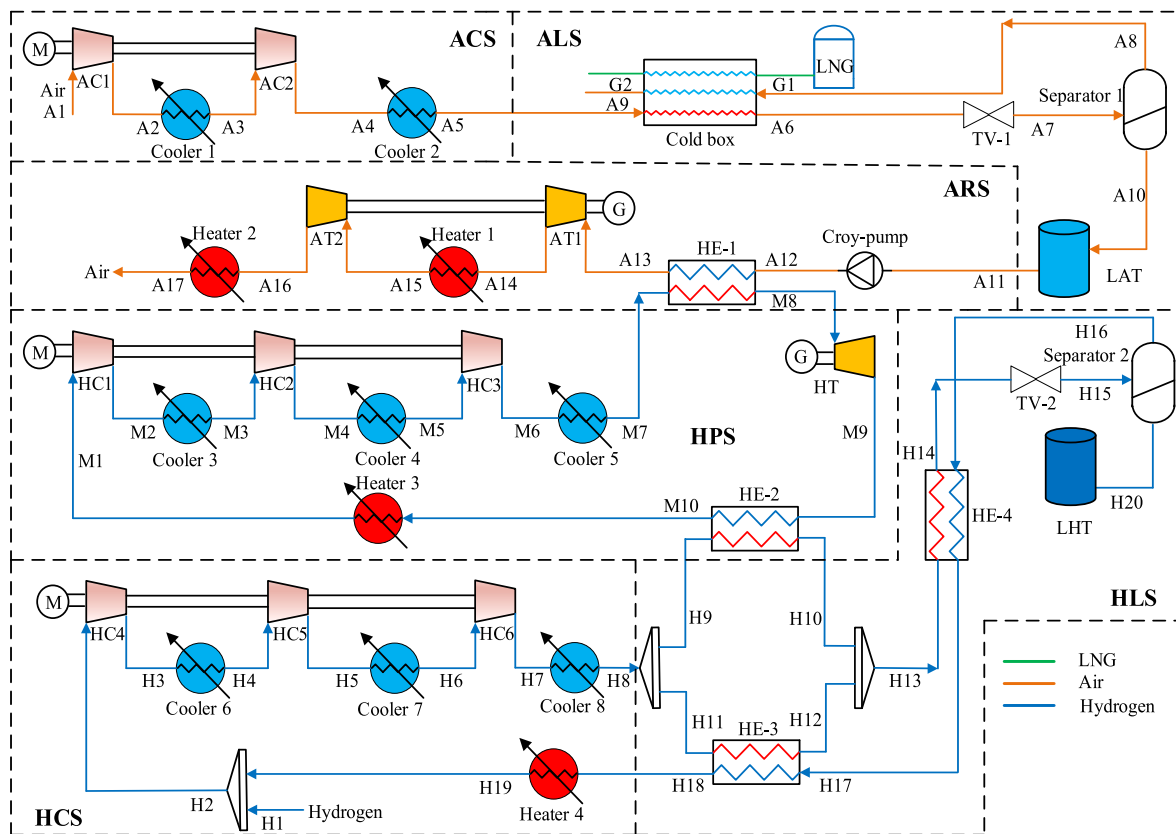


Fig. 3. Schematic diagram of the proposed LNG-LAES-LH₂ system.

consumption. At the same time, the hydrogen turbine can further reduce the refrigerant temperature to 27.75 K, and then feed it into the heat exchanger HE-2. Therefore, the cold energy of the pre-cooling system can be used in the hydrogen liquefaction system (HLS).

- (5) The hydrogen compression system (HCS) is mainly composed of the three-stage hydrogen compressors (HC4, HC5, HC6). The hydrogen generated by electrolysis passes into node H1, and the unliquefied hydrogen joins together through a confluence, and then through a three-stage hydrogen compressor and a condenser. Therefore, the room temperature atmospheric pressure air is converted into high-pressure room temperature air.
- (6) In the hydrogen liquefaction system (HLS), a part of the high-pressure room-temperature hydrogen passes through the heat exchanger HE-2 to absorb the cold energy. The other part of the hydrogen uses the cold energy of unliquefied hydrogen in the heat exchanger HE-3 for pre-cooling. After the pre-cooled high-pressure low-temperature hydrogen passing through the confluence, the cold energy of the unliquefied hydrogen exchanges in HE-4, and goes through the control valve TV-2. Finally, the high-pressure low-temperature hydrogen is converted into normal pressure liquid hydrogen, and is stored into liquid hydrogen tank.

3.2. Analysis tools and system assumptions

The LNG and air compositions are shown in Table 1. Table 2 shows the default operating parameters and basic settings for the LNG-LAES-LH₂ system. In addition to LNG and air, hydrogen was selected from Aspen HSHS and the classical Peng-Robinson equation was used for substances. The following assumptions were made for the LNG-LAES-LH₂ system:

Table 1
Compositions of LNG and air (Peng et al., 2019; Zhang et al., 2018).

Component		Mole fractions
LNG	Methane	91%
	Ethane	5%
	Propane	2.5%
	i-Butane	1%
	i-Pentane	0.1%
	Nitrogen	0.4%
Air	Nitrogen	78.12%
	Oxygen	20.96%
	Argon	0.92%

- There were no heat losses in pipelines and components.
- The pinch points temperature differences of the cold box and the heat exchanger were 5 K and 2 K, respectively (Liu et al., 2020; Yue et al., 2023).
- Only the pressure changes caused by compressors, expanders and control valves were considered, and the pressure losses from pipelines and other components were ignored.
- There were 12 h in both the peak and off-peak time.
- The isentropic efficiency of the compressor and turbine was 85% (Xin et al., 2022; Batlle et al., 2021).
- The system was in steady state.
- There was no leakage of medium (Peng et al., 2019).

3.3. Simulation result

Table 3 and Table 4 show the data of each node of the system. In the heat transfer process of the cold box, the cold energy provided by unliquefied low-temperature air accounts for about 21.6% of the total cold energy. The cold exergy of low-temperature air is higher than that

Table 2
Basic parameters of the LNG-LAES-LH₂ system.

Parameters	Values
Ambient pressure	101.3 kPa
Ambient temperature	298.15 K
Peak hours	12 h
Valley hours	12 h
Storage pressure of liquid air	0.1 MPa
Storage pressure of liquid hydrogen	0.1 MPa
Pinch point temperature of heat exchanger	2 K
Pinch point temperature of cold box	5 K
LNG inlet temperature	111.15 K
LNG outlet temperature	298.15 K
LNG inlet pressure	0.1 MPa
LNG outlet pressure	0.1 MPa
Air inlet temperature	295.15 K
Hydrogen inlet temperature	298.15 K
Pressure drop	0%
Heat leakage	0%
Isentropic efficiency of compressor	85%
Isentropic efficiency of turbine	85%
Isentropic efficiency of cryo-pump	85%
Operating pressure of hydrogen pre-cooling	10 MPa

Table 3
Thermodynamic parameters of LAES.

Stream	m (kg/s)	P (MPa)	T (K)	h (kJ/kg)	s (kJ/kg-K)	e (kJ/kg)
A1	54.28	0.1	298.15	-0.28	5.261	-1.131
A2	54.28	0.5	498.35	205.8	5.325	185.9
A3	54.28	0.5	298.15	-1.387	4.794	137
A4	54.28	3	527.25	235.1	4.863	352.7
A5	54.28	3	314.73	9.589	4.361	290.4
A6	54.28	3	112.45	-349.2	2.113	588.4
A7	54.28	0.1	79.05	-349.2	2.302	532.2
A8	18.95	0.1	79.05	-222.1	3.956	177
A9	18.96	0.1	298.15	-0.276	5.298	-1.149
A10	35.33	0.1	79.05	-417.5	1.414	715.1
A11	38.89	0.1	79.05	-417.5	1.414	715.1
A12	38.89	8	82.65	-406.6	1.453	719.4
A13	38.89	8	296.15	-22.17	3.916	369.3
A14	38.89	1	175.88	-127.6	4.028	230.6
A15	38.89	1	298.15	-2.77	4.567	194.7
A16	38.89	0.1	173.65	-123.4	4.698	34.97
A17	38.89	0.1	298.15	-0.28	5.232	-1.121
G1	17.37	0.1	111.15	-5137	4.218	956.5
G2	17.37	0.1	298.15	-4258	10.38	-1.811

of LNG, which means that the cold exergy of unliquefied low-temperature air can be fed back into the next round of air liquefaction, and the liquid air production will increase by more than 21.6%. At the same time, in the hydrogen liquefaction system, the unliquefied low-temperature hydrogen can also be fed back into the next round of liquefaction process, and the cold energy accounts for about 33.45% of the cold energy provided by the hydrogen pre-cooling system.

4. Modeling

4.1. Energy modeling

Based on the first law of thermodynamics, in the charging process, the power consumption of air compression is:

$$W_{air,c} = \frac{h_{A2} - h_{A1} + h_{A4} - h_{A3}}{\eta_{com}} \cdot m_{air,c} \quad (1)$$

where h is the specific enthalpy of each node, η_{com} is the isentropic efficiency of the compressor (85%), and $m_{air,c}$ is the mass flow rate of the charging process.

In 24 h, the power consumption of compressed air is:

Table 4
Thermodynamic parameters of LH₂ process.

Stream	m (kg/s)	P (MPa)	T (K)	h (kJ/kg)	s (kJ/kg-K)	e (kJ/kg)
M1	4.72	0.1	298.15	-0.053	61.07	-16.19
M2	4.72	0.4	472.15	2473	61.88	2216
M3	4.72	0.4	298.15	-0.201	55.35	1690
M4	4.72	2	507.15	2980	56.26	4399
M5	4.72	2	298.15	-0.686	48.68	3676
M6	4.72	10	507.75	3022	49.61	6423
M7	4.72	10	298.15	3.748	41.94	5691
M8	4.72	10	86.95	-3166	23.05	8152
M9	4.72	0.1	27.75	-3790	27.72	6136
M10	4.72	0.1	257.95	-566.2	59.03	25.75
H1	3.25	0.1	298.15	-0.053	61.07	-16.19
H2	4.8	0.1	298.15	-0.053	61.07	-16.19
H3	4.8	0.4	472.15	2473	61.88	2216
H4	4.8	0.4	298.15	-0.201	55.35	1690
H5	4.8	2	507.15	2980	56.26	4399
H6	4.8	2	298.15	-0.686	48.68	3676
H7	4.8	8	472.75	2509	49.5	5941
H8	4.8	8	298.15	1.658	42.88	5408
H9	3.64	8	298.15	1.658	42.88	5408
H10	3.64	8	31.15	-4175	4.102	12790
H11	1.16	8	298.15	1.658	42.88	5408
H12	1.16	8	31.15	-4175	4.102	12790
H13	4.8	8	31.15	-4175	4.102	12790
H14	4.8	8	27.55	-4224	1.96	13380
H15	4.8	0.1	18.65	-4224	5.675	12270
H16	1.55	0.1	18.65	-3922	21.88	7745
H17	1.55	0.1	29.05	-3771	28.39	5956
H18	1.55	0.1	252.62	-641	58.74	38.35
H19	1.55	0.1	298.15	-0.053	61.07	-16.19
H20	3.25	0.1	18.65	-4369	-2.07	14440

$$W_{air} = \sum_{k=1}^{24} W_{air,c} \quad (2)$$

where k is time.

The air liquefaction rate is [40]:

$$Y_{air} = \frac{m_{A10}}{m_{A1}} \quad (3)$$

where m is the mass flow, and the subscript represents the node.

In 24 h, the total amount of air liquefaction is:

$$M = \sum_{i=1}^{24} m_{A10} \quad (4)$$

The specific energy consumption of liquid air is:

$$SEC_{air} = \frac{W_{air}}{M} \quad (5)$$

The cold energy provided by LNG is:

$$W_{LNG} = \sum_{i=1}^{24} (h_{G2} - h_{G1}) \cdot m_{LNG} \quad (6)$$

The amount of air used in the re-gasification process is:

$$m_{air,d} = m_{A11} \cdot t_{valley} \quad (7)$$

where m_{A11} indicates the mass rate of node A11, and t_{valley} is the trough period (12 h).

In the air discharging process, the cryogenic pump consumes a part of the electricity and the turbine produces a part of the electricity. Finally, the net electricity generated is:

$$W_{air,g} = \left((h_{A14} - h_{A13} + h_{A16} - h_{A15}) \cdot \eta_{tur} - \frac{h_{A12} - h_{A11}}{\eta_{com}} \right) \cdot M_{air,d} \cdot t_{valley} \quad (8)$$

where η_{tur} is the isentropic efficiency of the turbine, and its value is 85%.

In general, the round-trip efficiency of liquid air energy storage is defined as the electric energy generated by the turbine over the electric energy consumed by the air re-gasification process. The liquid air cold energy in this paper is mainly used to liquefy hydrogen, so the electricity

generation is not significant. In this paper, the electricity consumption saved by the hydrogen liquefaction process is equivalent to the electricity generation generated by the air re-gasification process. Therefore, in this paper, the liquid air round-trip efficiency is defined as the sum of the power generated in the air re-gasification process and the electric energy saved by liquefied hydrogen, over the electric energy consumed in the air liquefaction process.

$$\eta_{LAES} = \frac{W_{air,g} + W_s}{SEC_{air} \cdot m} \quad (9)$$

where W_s is the electricity saved by the liquid air cold energy.

The hydrogen pre-cooling system is composed of a three-stage hydrogen compressor, a hydrogen turbine and multiple heat exchangers. Considering that the hydrogen turbine can produce a certain amount of power compensation, the total power consumption of the whole pre-cooling system is:

$$W_{int,c} = \left(\frac{h_{M2} - h_{M1} + h_{M4} - h_{M3} + h_{M6} - h_{M5}}{\eta_{com}} - (h_{M9} - h_{M8}) \cdot \eta_{tur} \right) \cdot m_{int} \cdot t_{valley} \quad (10)$$

where m_{int} is the mass flow rate of the hydrogen pre-cooling system.

The electricity consumption of hydrogen compression system is:

$$W_{hyd,c} = \frac{h_{H3} - h_{H2} + h_{H5} - h_{H4} + h_{H7} - h_{H6}}{\eta_{com}} \cdot m_{hyd} \cdot t_{valley} \quad (11)$$

The power consumption of the system is:

$$W = W - W_{air,g} + W_{int,c} + W_{hyd,c} \quad (12)$$

The hydrogen liquefaction rate can be calculated by:

$$Y_{hyd} = \frac{m_{H20}}{m_{H2}} \quad (13)$$

The specific energy consumption of liquid hydrogen is:

$$SEC_{hyd} = \frac{SEC_{air} \cdot M_{air,d} - W_{air,g} + W_{int,c} + W_{hyd,c}}{m_{H20} \cdot t_{valley}} \quad (14)$$

4.2. Exergy modeling

Exergy modeling is based on the first and second laws of thermodynamics, which mainly considers the degree of irreversibility of various processes in the system. Exergy analysis can accurately evaluate the perfection of the thermodynamics and the loss of a system. In general, the exergy of state i can be calculated by (Abd Elbar et al., 2019):

$$E_i = m_i \cdot [(h_i - h_0) - T_0(s_i - s_0)] \quad (15)$$

where m is mass flow rate, h is specific enthalpy, s is specific entropy, and subscripts i and s represent states and environmental conditions. T_0 is 298.15 K.

The equation of exergy can be expressed as (Park et al., 2020; Qi et al., 2020):

$$E_{in} = E_{out} + E_{x_{loss}} \quad (16)$$

where E_{in} and E_{out} represent the exergy of the inlet and outlet.

$$E_{in} = E_{x_{in}} + W_{in} \quad (17)$$

$$E_{out} = E_{x_{out}} + W_{out} \quad (18)$$

where $E_{x_{in}}$ and $E_{x_{out}}$ represent the exergy flows of the inlet and outlet, and W_{in} and W_{out} represent the electricity of the input and output.

The exergy efficiency of each sub-system, and the overall system can be calculated as follows (Dorosz et al., 2018):

$$\eta_{exe} = \frac{E_{out}}{E_{in}} \quad (19)$$

The exergy input and exergy output of each subsystem and the whole system are shown in Table 5.

5. System analysis and evaluation

5.1. Energy analysis

The selection of reasonable pressure in air liquefaction process is the key to air liquefaction process. Excessive air pressure will lead to excessive power consumption of the air compressor. If the air pressure is too low, the liquefaction temperature will be relatively low, which will lead to the cold energy of LNG cannot be fully used for air liquefaction pre-cooling, and eventually the liquefaction rate of air will be low. As shown in Fig. 4, the air liquefaction temperature increases with the increase of air pressure. Since the process of air from gas to liquid absorbs a large amount of cold energy while the temperature is almost unchanged, the air liquefaction temperature is higher than the LNG gasification temperature, which is conducive to the use of LNG cold energy for air liquefaction. At 2 MPa, the liquefaction temperature is about 118.45 K. Considering that the pinch-point temperature difference of cold-box is 5 K, only the cold energy of 111.15 K–113.45 K LNG can be used for air liquefaction. However, at 113.45 K, LNG only vaporized 52.85%, nearly 50% of LNG vaporized, and the cold energy released cannot be used for air liquefaction, which indicates that the pressure of 2 MPa is not high enough. Under the pressure of 3 MPa, the air liquefaction temperature is 127.25 K, and the cold energy below 122.25 K can be used in the air liquefaction process, and the gas phase ratio of LNG reaches 86.63%, so the pressure of 3 MPa will be more appropriate. Therefore, in this study, the air liquefaction pressures 3 MPa, 4 MPa, 5 MPa were selected for the comparative analysis.

The ratio of the LNG mass to the input air mass (m_{LNG}/m_{air}) has great influence on the parameters of each node in the air liquefaction system. Under a certain pressure, the lower the temperature of node A6 is, the greater the air liquefaction rate will be after passing through controller TV-1. Due to the influence of the temperature of the cold box pinch point, when the pressure of node A6 is determined and the m_{LNG}/m_{air} ratio is fixed, the lowest temperature that node A6 can reach will be determined. Afterwards, the air liquefaction rate and the mass flow rate of node A10 (m_{A10}) can be determined, as shown in Fig. 5.

According to Fig. 5, the pressure of the air compression system is 5 MPa and the m_{LNG}/m_{air} ratio is 0.12. At a given mass flow rate of LNG, the highest amount of liquid air is produced, but this ignores the electricity consumption of compressed air. A low m_{LNG}/m_{air} ratio leads to a high temperature of air node A6, resulting in a low liquefaction rate. A lot of air is compressed but not liquefied, resulting in a large amount of energy waste. In this work, a performance indicator of specific energy consumption (SEC) of liquid air is introduced to properly select the m_{LNG}/m_{air} ratio and air liquefaction pressure, as shown in Fig. 6.

Fig. 6 shows that when the m_{LNG}/m_{air} ratio is lower than 0.32, the electricity consumption per unit mass of liquid air generation decreases as the m_{LNG}/m_{air} ratio increases. This is mainly because when the ratio is small, the air mass flow is large, and the cold capacity of LNG is not enough to cool the air to a lower temperature, so after the air passing TV-1, the liquefaction rate is low. Second, when the ratio reaches 0.32, and continues to increase, the electricity consumption per unit mass of air

Table 5
Input and output of exergy of component.

Component	E_{in}	E_{out}
ACS	$W_{air,c}$	E_{A5}
ALS	$E_{G1} + E_{A5}$	E_{A10}
ARS	$E_{A11} + W_{c-p}$	$(E_{A12} - E_{A13}) + W_{air,g}$
HPS	$W_{h,c1} + (E_{A12} - E_{A13})$	$W_{h,g} + (E_{M9} - E_{M10})$
HCS	$W_{h,c2} + E_{H18} + E_{H1}$	E_{H8}
HLS	$E_{H8} + (E_{M9} - E_{M10})$	$E_{H18} + E_{H20}$
WS	$W_{air,c} + W_{c-p} + W_{h,c1} + W_{h,c2} + E_{G1}$	$W_{air,g} + W_{h,g} + E_{H20}$

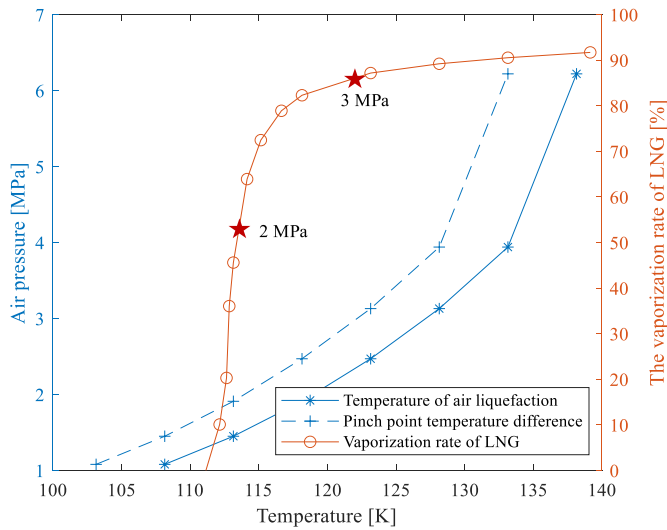


Fig. 4. Selection of air liquefaction pressure.

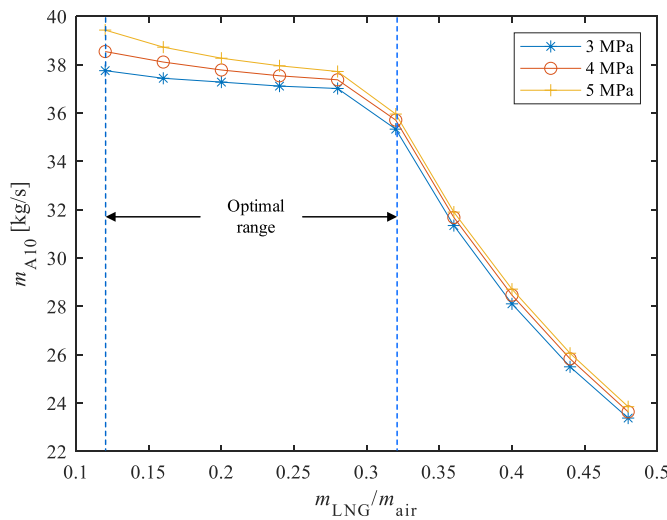


Fig. 5. Effect of m_{LNG}/m_{air} on m_{A10} .

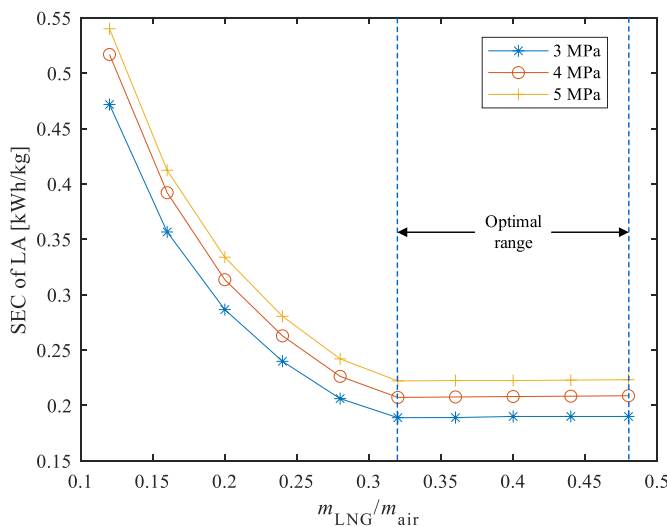


Fig. 6. Influence of m_{LNG}/m_{air} on SEC of LAES.

liquefied will be almost unchanged. This is mainly because of the temperature limit of the pinch point of the cold box, even if the mass flow rate of the air is reduced, the air cannot reach a lower temperature, so the air liquefaction rate remains almost unchanged. In the case of a certain m_{LNG}/m_{air} ratio, with the increase of node A4 pressure, the electricity consumption per unit mass of air liquefied will increase. Using the intersection of the two optimal regions in Figs. 5 and 6, the optimal m_{LNG}/m_{air} ratio of 0.32 and pressure of 3 MPa can be selected. Under this condition, the temperature of node A6 is 112.4 K, the air liquefaction rate is 64.49%, the mass flow rate of node A10 is 35.33 kg/s, and the power consumption per unit mass of liquid air is 0.189 kWh/kg.

In the heat exchanger HE-1, after heat exchange with liquid air (node M8), the lower the temperature of the refrigerant is in the hydrogen pre-cooling system, the lower the temperature (T_{M8}) can reach after the expansion of the hydrogen turbine. This consequence can provide lower temperature cold energy for the hydrogen liquefaction system. However, the lower the temperature of node M8 is, the lower the temperature of node A13 (T_{A13}) will be, and the cold energy of liquid air cannot fully enter the air pre-cooling system, resulting in less hydrogen liquefaction.

As shown in Fig. 7, when the temperature of node M8 decreases from 87.15 K to 86.95 K, the temperature of node A13 only slightly changes, so it is more appropriate for node M8 to adopt a lower temperature of 86.95 K. However, as the temperature of node M8 decreases, the temperature of node A13 decreases greatly, and the liquid air cooling energy cannot be well utilized. Therefore, it is not appropriate to further reduce the temperature of node M8, and thus the optimal temperature of node M8 is 86.95 K. Under this condition, the mass flow rate of node M8 is 4.72 kg/s, and the temperature of node A13 is 296.15 K.

In general, under the same pressure, the lower the temperature is before hydrogen expansion, the higher the hydrogen liquefaction rate will be. In order to determine the pressure of hydrogen liquefaction system, the temperature of node H14 was first selected as 37.15 K, 35.15 K, 33.15 K, 31.15 K and 29.15 K, respectively, to explore the influence of different pressures on the hydrogen liquefaction rate. As shown in Fig. 8, liquefaction rate increases first and then decreases with the increase of pressure in the range between 3 and 10 MPa. When the temperature of node H14 is 37.15 K and the pressure of node H14 is 8 MPa, the liquefaction rate reaches the highest. When the temperature of node H14 is 29.15 K and the pressure of node H14 is 4 MPa, the liquefaction rate is the highest. This means that the pre-expansion temperature ranges from 37.15 K to 29.15 K, and the maximum pressure ranges from 4 MPa to 8 MPa. In order to determine the optimal pressure of hydrogen liquefaction system, 4 MPa, 6 MPa and 8 MPa were selected for case studies in this paper.

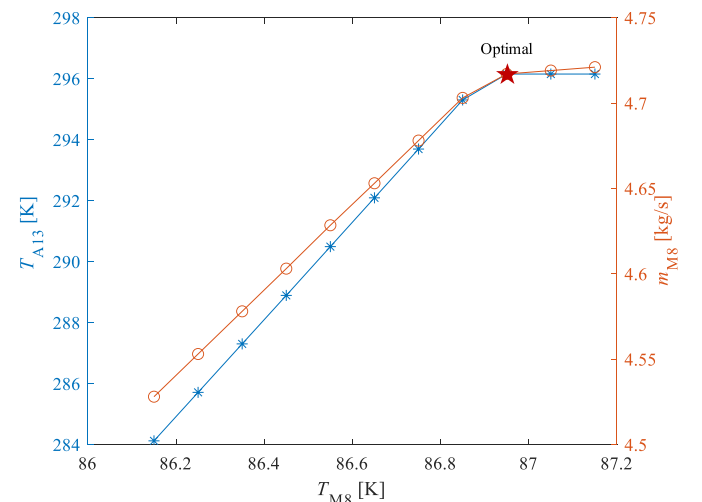


Fig. 7. Effect of T_{M8} on m_{M8} and T_{A13} .

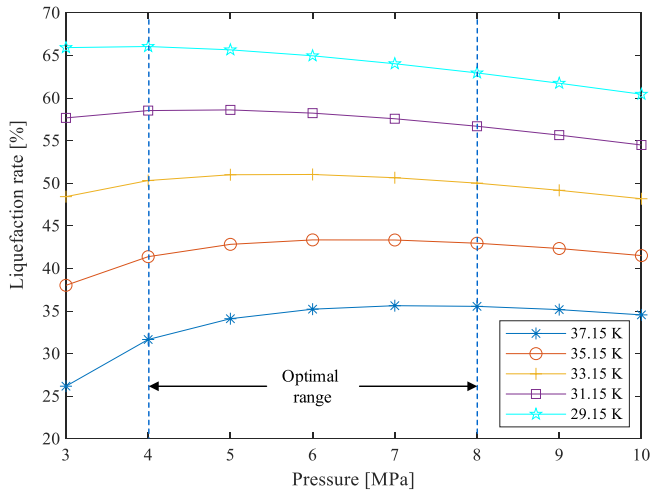


Fig. 8. Effect of different temperature and pressure on hydrogen liquefaction rate.

The hydrogen liquefaction rate is not only affected by the node H14 pressure, but also by the temperature. In the hydrogen liquefaction system, the temperature of high-pressure hydrogen is set to be the same after the heat exchange and pre-cooling of the heat exchanger HE-2 and HE-3 (node H10 and node H12). When the temperature of node H10 is given, the lowest possible temperature that node H14 is also determined, so that the hydrogen liquefaction rate and hydrogen liquefaction amount (m_{H20}) can be determined. Fig. 9 shows the relationship between the amount of hydrogen liquefaction and the temperature (T_{H10}) of node H10.

For the LNG-LAES-LH₂ system, during the LAES process, when the pressure is 3 MPa and the m_{LNG}/m_{air} ratio is 0.32, the energy consumption of liquid air per unit mass is the lowest, which is 0.189 kWh/kg. Then the production of 1.4×10^5 kg of liquid air requires 26.46 MWh of electricity. Considering the electricity consumption of the hydrogen liquefaction process, the electricity consumption of the entire hydrogen liquefaction system is shown in Fig. 10.

According to the electric energy consumed by the system in Fig. 10 and the output of liquid hydrogen in Fig. 9, the curve correlating the specific energy consumption (SEC) of liquid hydrogen and the temperature of node H10 (T_{H10}) can be plotted, as shown in Fig. 11. It shows that when the temperature of node A10 is 31.15 K and the pressure is 8

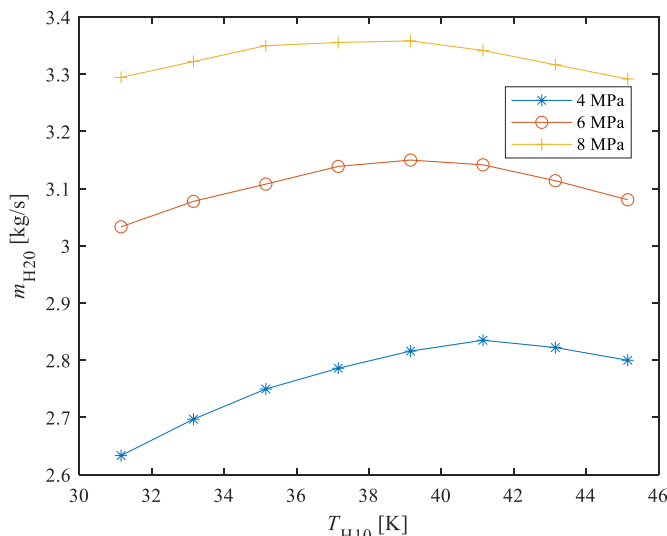


Fig. 9. Effect of T_{H10} on m_{H20} .

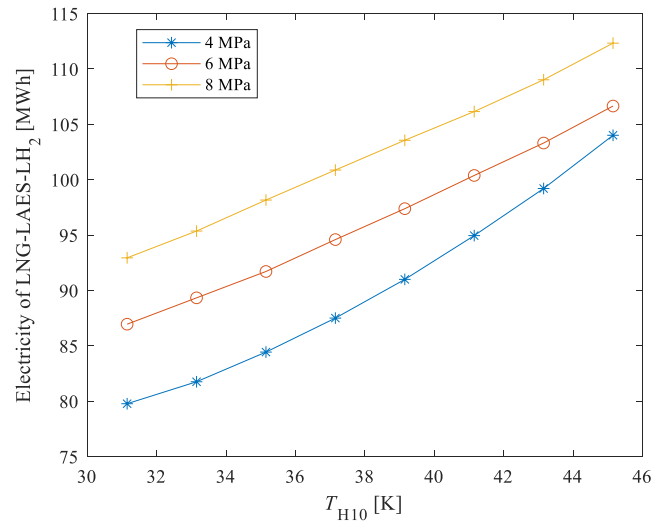


Fig. 10. Effect of T_{H10} on power consumption of LNG-LAES-LH₂.

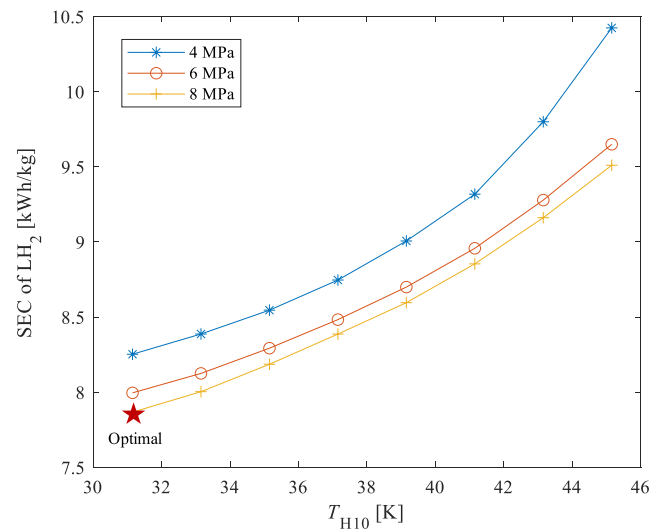


Fig. 11. Effect of T_{H10} on SEC of LH₂.

MPa, the SEC of LH₂ is the lowest, about 7.87 kWh/kg.

5.2. Exergy analysis

Fig. 12 shows the exergy loss and exergy efficiency of various subsystems. The exergy loss of hydrogen pre-cooling system reaches the maximum of 943.3 GJ, accounting for 32.28% of the total exergy loss. The exergy efficiency is also the lowest hydrogen pre-cooling system, 59.26%. This is mainly because when the heat generated during the process of compressing, the refrigerant is not properly utilized.

The exergy flow of the LNG-LAES-LH₂ system is calculated, as shown in Fig. 13. The exergy input is 5456.8 GJ, exergy output is 2534.2 GJ, exergy loss is 2922.6 GJ, and system exergy efficiency is 46.44%. The exergy of 4,669.2 GJ enters in the form of electrical energy, accounting for 85.57% of the total input, while the rest of exergy is imported by LNG cold exergy. 2027.4 GJ outputs in the form of liquid hydrogen, accounting for about 80% of the total output, and the rest outputs in the form of electrical energy.

The exergy input of LAES is 2077.3 GJ, of which the electrical energy is 1289.7 GJ, accounting for about 62.09% of LAES input. Exergy in cold energy and electrical energy are 588.2 GJ and 379.8 GJ, respectively. As

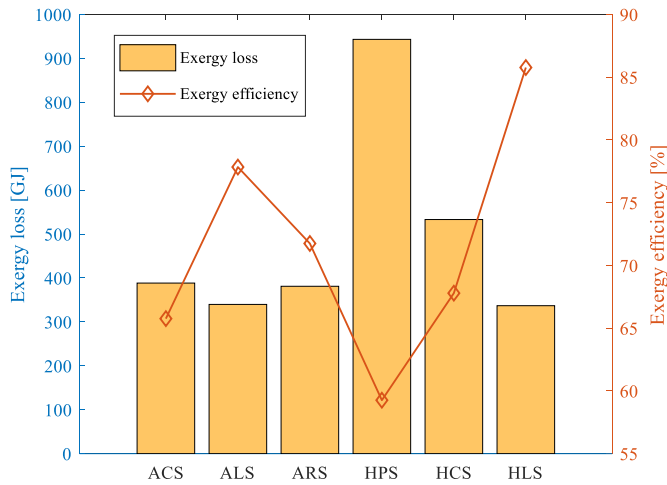


Fig. 12. Exergy loss and exergy efficiency of the six subsystems.

a result, the LAES has an exergy efficiency of 46.6%.

In this paper, when the air pressure is 3 MPa and the m_{LNG}/m_{air} ratio is 0.32, the maximum ratio of the electric energy generated by the air re-gasification process over the electric energy consumed by the air liquefaction process is 43%. The cold energy of liquid air is used to prepare liquid hydrogen, which is not used for power generation such as Rankine cycle. Therefore, the electricity saved by the hydrogen liquefaction process can be equivalent to the electricity generated by liquid air. When the liquid air cooling energy is not utilized, the specific energy consumption of liquid hydrogen is 8.5 kWh/kg (Zhang et al., 2023). In the system of this paper, the specific energy consumption of liquid hydrogen is 7.87 kWh/kg, and the electricity consumption reduces by 0.63 kWh per kilogram of liquid hydrogen. Since the ratio of liquid air

consumption over liquid hydrogen production is 11.97, the proposed system can save 0.053 kWh/kg of liquid air. Since the liquid air energy storage process consumes 0.189 kWh/kg, the ratio of the energy saved per kg of liquid air over the energy consumed by the energy storage process is 28.0%.

Fig. 14 shows the round-trip efficiency of the system. When the m_{LNG}/m_{air} is 0.12, the round-trip efficiency gradually increases with the increase of the ratio. When the ratio is 0.32 and continues to increase, the round-trip efficiency will remain unchanged. This is mainly because when the ratio is low, the power generation of liquid air per unit mass remains unchanged, but the air liquefaction rate is low, and the power consumption of liquefied air per unit mass is larger. When the ratio is high, the liquefaction rate will remain constant, and the electricity consumption per unit mass of liquid air generated will remain, so the round-trip efficiency will remain almost constant at the ratio of 0.32–0.4. Combined with Fig. 6, during the air liquefaction process, the specific energy consumption of liquefied air is the lowest when the air pressure is 3 MPa. Under such conditions, the optimal round-trip efficiency of liquid air is about 71.0%. Correlating to Fig. 6, during the air liquefaction process, with the m_{LNG}/m_{air} ratio 0.32, the energy consumption of air liquefaction reaches the lowest. Considering the liquid air round-trip efficiency and the best range of specific energy consumption, in this article the m_{LNG}/m_{air} ratio was set as 0.32, with round-trip efficiency 71.0% and specific energy consumption 0.189 kWh/kg.

5.3. Case analysis

The natural gas load curve and liquid hydrogen consumption curve of a typical day are drawn according to the example in literature (Gong et al., 2014), as shown in Figs. 15 and 16 (orange, triangle). By combining LNG cold energy and surplus offshore wind power to produce liquid air, the output of liquid air will be basically consistent with the change of natural gas load. Because offshore surplus wind power is more

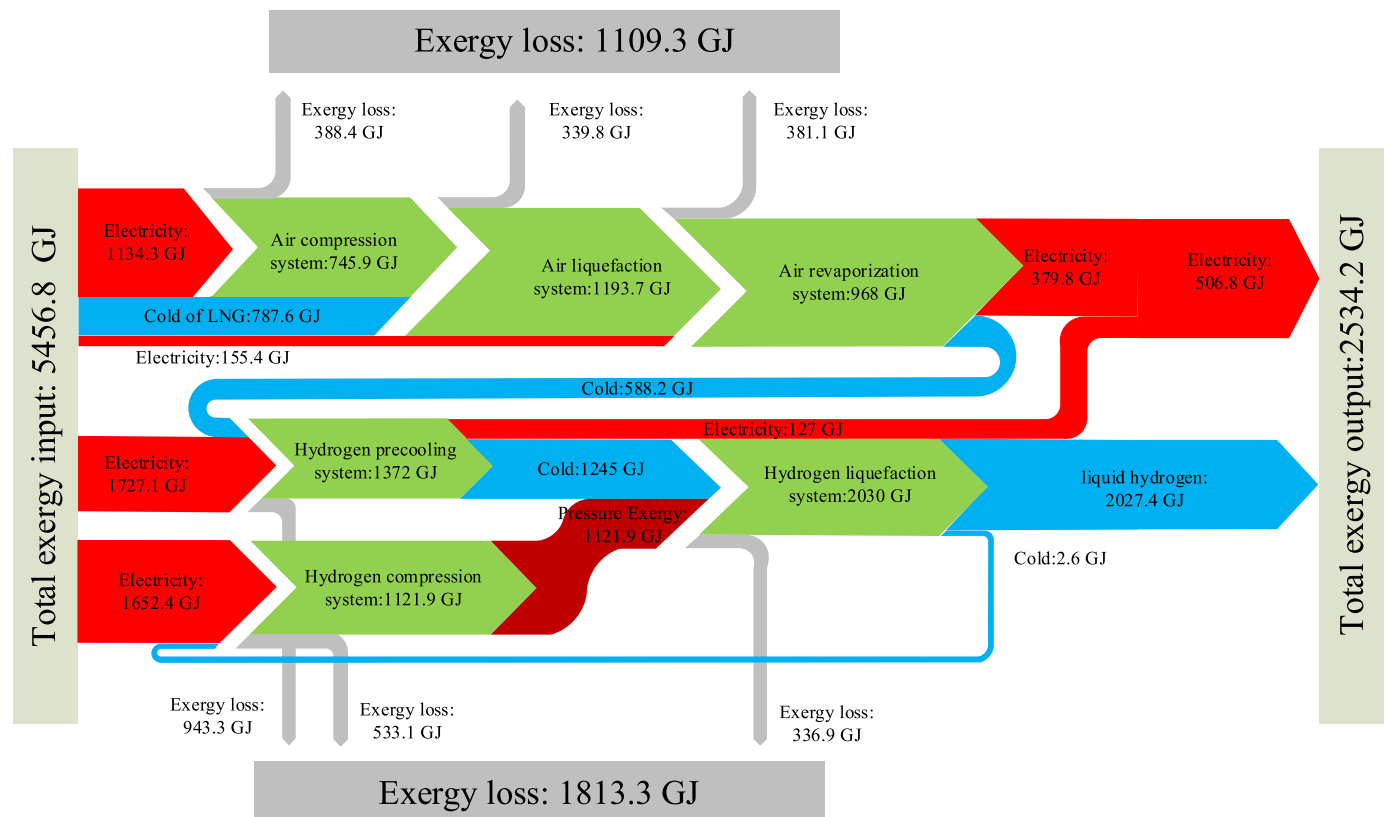


Fig. 13. Exergy analysis of the LNG-LAES-LH₂ system.

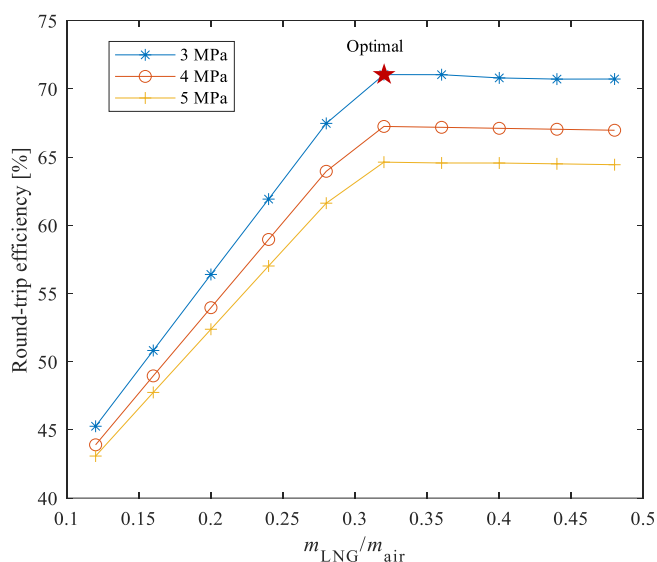


Fig. 14. Effect of m_{LNG}/m_{air} on air round-trip efficiency.

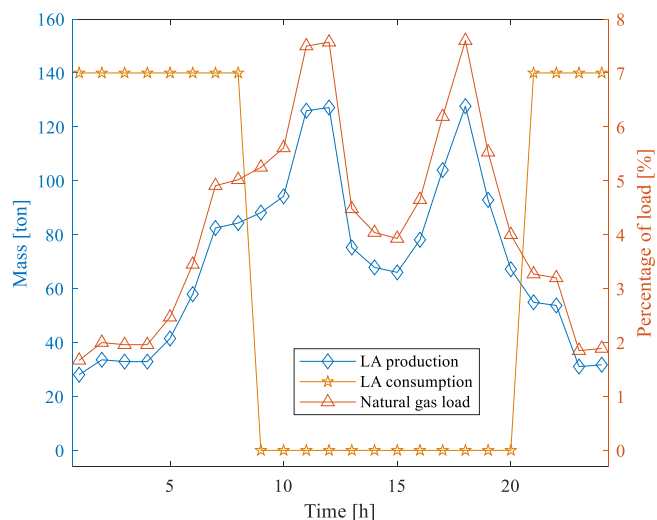


Fig. 15. Percentage of natural gas load and liquid air production and consumption.

at night and less during the day, the ratio of nighttime hydrogen production to daytime electrolytic hydrogen production can be set as 3:1. The hydrogen liquefaction is operated at night, and liquid hydrogen is prepared by using liquid air cold energy and surplus offshore wind power. The output of liquid hydrogen is proportional to the consumption of liquid air. In the case study, the air liquefaction process and the hydrogen liquefaction process operate with the node optimization parameters obtained in Figs. 4–11 to minimize the specific energy consumption of the air liquefaction process and the hydrogen liquefaction process.

Fig. 15 shows the amount of liquid air produced and consumed. During 18:00 to 19:00, the maximum natural gas load rate is 7.6% and liquid air production was 127.68 tons. The total liquid air production was 1680 tons in 24 h. Liquid air will be used for the production of liquid hydrogen at night, with the average consumption of 140 tons per hour, and the total preparation time of liquid hydrogen is 12 h. The total consumption of liquefied air is 1680 tons, and the production and consumption have dynamic balance every day.

Fig. 16 shows hydrogen production, liquid hydrogen production, and

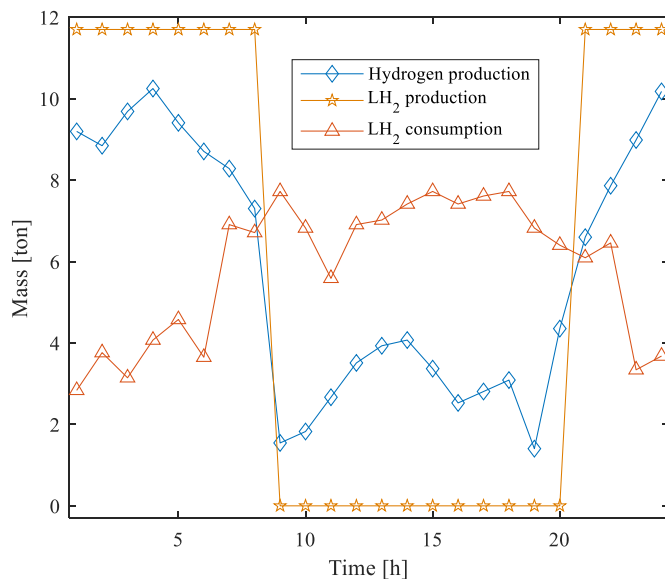


Fig. 16. Liquid hydrogen production and consumption and existing hydrogen production.

consumption. During the period from 4:00 to 5:00, the highest hydrogen production is 10.25 tons, and the cumulative hydrogen production throughout the day is 140.4 tons. The hydrogen produced liquefies at a rate of 11.7 tons per hour at night. Liquid hydrogen is consumed in the whole day, with the largest consumption of 7.722 tons from 9:00 to 10:00. In 24 h, the cumulative consumption is 140.4 tons, maintaining the production of liquid hydrogen with dynamic equilibrium.

Fig. 17 shows the power consumption during the air liquefaction process, hydrogen liquefaction process and electrolytic hydrogen production, as well as the total power consumption. The electricity consumption during the air liquefaction process and the hydrogen liquefaction process is proportional to the percentage of natural gas load and the amount of liquid air used. From 18:00 to 19:00, the maximum power used in the air liquefaction process is 24.02 MW. The electricity power of hydrogen liquefaction process is 78.59 MW, and the power generation of air turbine 1, air turbine 2 and hydrogen turbine is 4.101 MW, 4.691 MW and 2.943 MW, respectively. The generated electricity will compensate the consumption from the hydrogen liquefaction process, and the electricity consumption of hydrogen liquefaction process

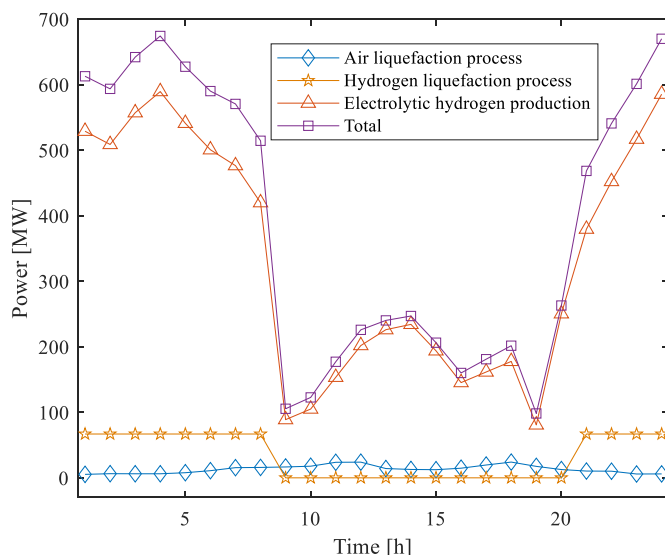


Fig. 17. Electric loads during a typical day.

after compensation is 66.855 MW. Electrolytic hydrogen production was considered to be 17.39 kg/MWh (Chen et al., 2023), and the power consumption of electrolytic hydrogen production was calculated. The total power of the system can be calculated by the electric power during the air liquefaction process, hydrogen liquefaction process and electrolytic hydrogen production process. From 4:00 to 5:00, the electric power and total electricity for electrolytic hydrogen production reach the maximum, which are 589.373 MW and 674.2 MW.

In this operation mode, in 24 h, the electrolytic production of 140.4 tons of hydrogen consumes 8.074 GWh. 140 tons of liquefied hydrogen will vaporize 821.92 tons, and the electricity consumption of liquid hydrogen liquefaction process is 1.118 GWh, and the total electricity consumption is 9.192 GWh.

Based on the case study above, by dynamically controlling the liquid air production/liquefaction, the unstable cold energy from LNG gasification can be efficiently stored, which can be used for hydrogen liquefaction. By using the new scheme of electrolytic hydrogen production together with liquid air liquefaction, stable hydrogen production can be powered by unstable off-shore wind energy, which realizes a high round-trip efficiency and low specific energy consumption. During daily operation, 24-h liquid air storage can achieve dynamic equilibrium, and satisfy the energy output requirement of liquid hydrogen, LNG, and clean electricity, which proves the feasibility and practicality of the proposed LNG-LAES-LH₂ scheme.

5.4. General design guideline

Besides Hainan Province, other regions in China and other countries with the similar characteristics (LNG receiving stations are close to the off-shore wind farms) can also use wind energy and LNG cold energy to produce LH₂. In 2022, the imported LNG in China reached 63.44 million tons (General Administration of Customs, People's Republic of China, 2023), which was mainly received, gasified, and stored by tens of LNG receiving stations.

There are several candidates of regions where this technology can be used. For examples, in China, there is a 22 GW off-shore wind farm in Guangdong Province, with 12 GW in East Guangdong, and 10 GW in West Guangdong (People's Government of Guangdong Provincial, 2021). There is a LNG receiving station to be built in 2024, in Yangjiang, Guangdong Province, which will be close to the 22 GW off-shore wind farm (Yangjiang City natural resources Bureau high-tech distribution, 2023). There is also a LNG receiving station with annual LNG production of 6.5 million tons, which is also close to the 22 GW off-shore wind farm (State-owned Assets Supervision and Administration Commission of Guangdong Provincial People's Government, 2022). In Shandong province, there is a 10 GW off-shore wind farm, and its capacity will increase to 35 GW in 2030, where this project will come across 3 major cities of Weihai, Yantai, and Dongyin (Energy Bureau of Shandong Province, 2023a,b). The LNG receiving station at Yantai has the maximum receiving capacity of 5.9 million tons per year, which is also near the off-shore wind farm (Energy Bureau of Shandong Province, 2023a,b).

The general design procedures of the green LH₂ production using off-shore wind energy and LNG cold energy can be summarized as follows:

- (1) In HYSYS software, the Peng-Robinson equation is used. The model of liquid air production using LNG cold energy is built based on the optimization processes in Figs. 4–6. By using equations (1)–(6) and the model, the consumptions of electricity and LNG to produce a unit of liquid air can be obtained.
- (2) The amounts of the air being liquefied and the energy consumption can be obtained after the local fluctuations of the natural gas load are input into the model.
- (3) Combining the optimization processes in Figs. 7–11, the model of LH₂ production by LNG cold energy is built. By using equations

(8)–(14) and the model, the consumptions of electricity and liquid air to produce a unit of LH₂ can be obtained.

- (4) The liquid air produced in step (2) is input into the model in step (3). By using equation (7) and the model, the consumptions of electricity and liquid air, as well as the hydrogen being liquefied, can be obtained. Afterwards, the key parameters such as the LH₂ storage capacity, the power ratings of hydrogen compressor 1 and compressor 2, can be obtained.
- (5) The energy consumptions in step (2) and step (4), and the surplus off-shore wind energy are input into the model. The electricity for electrolytic hydrogen production can be obtained, and the operating capacity of electrolytic cells and the storage capacity of hydrogen tanks can be obtained.
- (6) After the model optimizations in step (1) and step (3), the optimal parameters for each critical node can be obtained. By using equations (15)–(19), the system specific energy consumption and the exergy efficiency can be obtained.

5.5. System performance comparisons

The proposed LNG-LAES-LH₂ scheme has the advantage that it uses the atmospheric pressure to produce hydrogen, which needs to complete the pressurization, pre-cooling, and liquefaction processes to reach the final LH₂ state. However, for most existing studies regarding the LH₂ production using clean power, LNG cold energy and liquid air, they use relatively high-pressure hydrogen as the input and then convert to the liquid state. A typical pressure of input hydrogen is 2.1 MPa. Due to various states of hydrogen near the input, the performance of hydrogen liquefaction (e.g., specific energy consumption, and exergy efficiency) cannot be directly compared with the data in this study. Therefore, in order to evaluate the technical advantages of the proposed LNG-LAES-LH₂ scheme, in this section the same input hydrogen pressure as the literatures is used, and then the model can calculate the final results.

When the 2.1 MPa input hydrogen goes through node H1 in Fig. 3, all the technological processes are the same as that of 0.1 MPa input hydrogen, except for the hydrogen compression subsystem. The technological processes of hydrogen compression subsystem are:

First, the normal-pressure unliquefied hydrogen from the previous liquefaction cycle at H19 is pressurized to 2.1 MPa via 3-stage compression, and then at the node H1 (combiner) it merges with the 2.1 MPa input hydrogen in another branch. Finally, the 2.1 MPa hydrogen at node H2 is further pressurized to 8 MPa for the subsequent liquefaction process.

Currently several studies show that the specific energy consumption of LH₂ can be greatly reduced if the liquefaction process of hydrogen can use extra cold energy. Generally, the lower temperature of extra cold energy is used, the less specific energy consumption will be. Table 6 and Table 7 summarize the typical system performance and results of using LNG cold energy to assist the production of LH₂ and liquid air.

The technical strategy of the proposed LNG-LAES-LH₂ firstly uses the unstable LNG cold energy to produce liquid air to store stable energy for

Table 6
Comparison with other studies on LH₂ using LA cold energy.

Publications	Cold source	State of the hydrogen input	SEC of HLP (kWh/kgLH ₂)	EXE of HLP (%)
Naquash et al. (2022)	LA	298 K 2.1 MPa	6.71	35.7%
Taghavi et al. (2021)	LA	298 K 2.1 MPa	5.955	52.9%
Riaz et al. (2021)	LA	298 K 2.1 MPa	8.52	N/A
Yang et al. (2023)	LA	298 K 2.1 MPa	7.25	53.2%
This paper	LA	298 K 2.1 MPa	5.04	55.56%

Table 7
Comparison with other studies on LH₂ using LNG cold energy.

Publications	Cold source	State of the hydrogen input	SEC of HLP (kWh/kgLH ₂)	EXE of HLP (%)
Riaz et al. (2021)	LNG	298 K 2.1 MPa	7.64	42.25%
Yang et al. (2019)	LNG	300K 2 MPa	11.05	N/A
Bae et al. (2021)	LNG	300K 2 MPa	10.26	N/A
Faramarzi et al. (2021)	LNG	300K 2 MPa	8.85	47%
This paper	LNG	298 K 2.1 MPa	7.31	49.34%

re-utilization, and then uses the valley electricity from off-shore wind farm and the cold energy from liquid air to produce LH₂. Results show that using the liquid air cold energy to liquefy LH₂ leads to a specific energy consumption 5.04 kWh/kg and exergy efficiency 55.56%, while using the LNG cold energy to liquefy LH₂ leads to a specific energy consumption 7.31 kWh/kg and exergy efficiency 49.34%. Tables 6 and 7 clearly prove that our proposed system has the technical merits of low energy consumption and high exergy efficiency.

The reasons for the lower specific energy consumption and higher exergy efficiency of the system put forward in this paper are as follows.

- (1) The low temperature cold energy of LNG is introduced to reduce the air liquefaction pressure to a smaller value, e.g., 3–5 MPa, effectively reducing the electricity consumption of air compression.
- (2) Considering the utilization rate of LNG cold energy and the range of air pre-cooling temperature, this paper optimally matched the proportion of LNG and air mass (m_{LNG}/m_{air}), e.g., 0.32. On the one hand, the rational utilization of LNG cold energy was maximized, and on the other hand, the specific energy consumption reduction of liquid air was effectively reduced, e.g., 189 kWh/kg.
- (3) By introducing the expansion link of hydrogen turbine, on the one hand, the refrigerant in the hydrogen pre-cooling system can generate certain electric energy, and on the other hand, the refrigerant can be reduced from 86.95 K to 27.75 K, providing cold energy at lower temperature for node H9.
- (4) The unliquefied low-temperature hydrogen gas adopts a two-stage heat transfer mode. By adjusting the pinch point temperature area of the original single-stage heat exchanger, the temperature of node H14 is effectively reduced.
- (5) After (3) and (4), the hydrogen liquefaction rate can be improved effectively, the amount of hydrogen for repeated compression can be reduced, and then the electricity consumption of compression system and the specific energy consumption of LH₂ can be reduced.

6. Economic analysis and benefit prediction

6.1. Economic model

In this paper, the net present value and investment payback period are two main indicators for analysis. The net present value is the difference between the present value of future capital inflows and the present value of future capital outflows. Considering the cumulative value over many years, the specific calculation is (Chen et al., 2023):

$$NPV = \sum_{x=1}^n \frac{P_x}{(1+j)^x} - C_{ii} \quad (20)$$

where j is the discount rate, whose value is 5%, and n is the production time. C_{ii} is the initial investment and P_x is the profit in year x , which can

be calculated:

$$C_{ii} = C_{EC} + C_C + C_{CB} + C_{HE} + C_{CT} + C_{LAP} + C_{LAT} + C_{LHT} + C_{AP} \quad (21)$$

$$P_x = P_{x,in} - P_{x,out} \quad (22)$$

where C_{EC} , C_C , C_{CB} , C_{HE} , C_{CT} , C_{LAP} , C_{LAT} , C_{LHT} and C_{AP} are electrolytic cell, compressor, cold box, heat exchanger, cryogenic turbine, liquid air pump, liquid air tank, liquid hydrogen tank and gas hydrogen tank. $P_{x,in}$ and $P_{x,out}$ are the revenue of year j and the operation and maintenance cost of year j , which can be calculated:

$$P_{x,out} = D_{EC} + D_{MC} + D_{OLC} + D_{MLC} + D_I \quad (23)$$

$$P_{x,in} = m_{H20} * t_{valley} * P_{LH2} \quad (24)$$

where m_{H20} is the mass flow rate of node H20 and P_{LH2} is the selling price of liquid hydrogen. D is expenditure, D_{EC} , D_{MC} , D_{OLC} , D_{MLC} and D_I are electricity, maintenance, operation labor, maintenance labor and insurance.

The dynamic payback period is the total time required for the net operating cash flow of an investment project to pay off the original total investment. It takes account the time cost and interest. It can be calculated by (Chen et al., 2023):

$$\sum_{x=1}^{DPP} \frac{P_x}{(1+j)^x} = C_{ii} \quad (25)$$

6.2. Hydrogen production model and economic parameters

If all the hydrogen is produced by valley electricity, this hydrogen production model will not require hydrogen storage tanks, and the hydrogen generated by electrolysis will be transported directly through pipelines to the hydrogen compression system and then will be liquefied. Considering the high cost of the electrolytic cell and its high electricity cost, the initial investment will be high. Therefore, this paper carries out the economic analysis on hydrogen production using 3 modes:

- 1) Mode 1: 100% hydrogen production is by valley electricity.
- 2) Mode 2: 25% hydrogen production is by peak electricity, and 75% hydrogen production is by valley electricity.
- 3) Mode 3: 50% hydrogen production is by peak electricity, and 50% hydrogen production is by valley electricity.

To efficiently reduce the capacity of electrolytic cells and the investment cost, the ratios of peak electricity and valley electricity are set 50% and 50% to produce hydrogen, but this strategy increase the operating cost. in order to balance the investment cost and operating cost, the ratios of peak electricity and valley electricity can also be set 25% and 75%, and the corresponding economic analysis and future estimation are carried out. the mode 1 and mode 3 are two extreme cases, and they can be modified by the prices of peak electricity, valley electricity, electrolytic cells, and hydrogen storage tanks in various practical applications.

The initial investment of the three hydrogen production modes is the same except for the initial investment of the electrolytic cell and the hydrogen storage tank. The three modes of hydrogen production, electrolytic cell and hydrogen storage tank capacity are shown in Table 8.

Table 8
Capacity of equipment for three hydrogen production modes.

	Mode 1	Mode 2	Mode 3
Schemes	100% VE	75% VE+25% PE	50% VE+50 PE
PEMEC	678.2 MW	508.7 MW	339.1 MW
GHT	0 t	35.1 t	70.2 t

The main economic parameters of the initial investment are shown in Table 9. The initial investment costs of the electrolytic cell under the three modes are 899.3, 674.5, 449.6 M\$, respectively. The initial investments of the hydrogen storage tank are 0, 54 and 108 M\$, respectively. The total initial investments are 923.1 M\$, 752.2 M\$ and 581.1 M\$, respectively.

The economic parameters and operating costs are shown in Table 10. The hydrogen in mode 1 comes from valley power, so its electricity cost is the lowest. The price of peak power and valley power is calculated at 0.07 \$/kWh and 0.04 \$/kWh, respectively. The total electricity costs of the three modes of hydrogen production and the liquefaction process are 136.5 M\$, 158.6 M\$ and 181 M\$, respectively. The maintenance costs are 42.5 M\$, 34.6 M\$ and 26.7 M\$, respectively. The annual operating costs are 179 M\$, 193.2 M\$ and 207.7 M\$, respectively.

From the analysis of initial investment and operating costs, the cumulative net present values of the three hydrogen production modes are shown in Fig. 18. Fig. 19 is a comparison of the initial investment, cumulative net present value and dynamic payback period of these three modes. Compared with mode 1, the initial investment, the NPV and DPP in mode 2 are 18.5%, 3.5% and 7.2% lower. Compared with mode 2, these three indicators of mode 3 are 22.7%, 4.7% and 10.8% lower. It can be seen that when the initial investment significantly reduces, the DPP and NPV are not reduced much. Therefore, the mode 3 is more economical.

6.3. Prediction of future economic

In this paper, the initial investment of electrolytic cell is large, but the cost of electrolytic cell will reduce with the maturity of technology in the future. At the same time, with the development of hydrogen production technology, the price of liquid hydrogen will also decrease, which is expected to be reduced to \$4/kg in 2050 (Di Micco et al., 2021). The design price will show a linear decline. As a result, the economical status of hydrogen production and liquefaction from offshore wind power will also change.

The relationship between the cost ($C_{EC,t}$, \$/kW) of the electrolytic cell and the time ($X_{EC,t}$, year) can be expressed as (Fusaro et al., 2020):

$$C_{EC,t} = 1.055 * (2.2998e + 60)e^{-0.06534X_{EC,t}} \quad (27)$$

The initial investment cost of the electrolytic cell and the selling price of liquid hydrogen are shown in Fig. 20. In 2035, the price of the electrolytic cell is 464.4 \$/kW and the selling price of liquid hydrogen is 4.75 \$/kg. The initial investment cost of the electrolytic cell in 2050 is 174.3 \$/kW, and the liquid hydrogen is sold at 4 \$/kg.

Fig. 21 analyzes the initial investment of three modes of electrolytic hydrogen production. It can be found that the initial investment of the three operating modes decreases with time, and the initial investment of mode 1 decreases most significant. Around 2040, the initial investments of the three models are relatively close, at 251 M\$, 248.2 M\$ and 245.4 M\$, respectively. Mode 3 has the smallest initial investment before 2040, and mode 1 has the smallest initial investment after 2040. This is

Table 9
Parameters of the initial investment.

Publications	Equipment	Cost model	Value (M\$)
Fusaro et al., 2020	PEMEC	1326 \$/kW	899.3/674.5/449.6
Couper et al. (2009)	Compressor	$7900(W)^{0.62}$ \$	10.08
Smith (2005)	Cold box	$32800(\frac{A}{80})^{0.68}$ \$	0.38
Akikur et al. (2014)	Heat exchanger	$130(\frac{A}{0.093})^{0.78}$ \$	0.13
Wu et al. (2020)	Cryo-turbine	$1100(W)^{0.81}$ \$	2.18
Park et al. (2021)	LAP	483 \$/kW	0.17
Gao et al. (2021)	LAT	320 \$/m3	0.59
Reddi et al., 2017	LHT	73 \$/kg	10.25
Chen et al. (2021)	GHT	1538 \$/kg	0/54/108

Table 10
Parameters of economic and operating cost.

Publications	Economic assumptions and cost parameters	Value
Haacker et al. (2020)	Plant operating life	20 years
	Discount rate	5%
Luo et al. (2020)	Peak power	0.07 \$/kWh
Luo et al. (2020)	Valley power	0.04 \$/kWh
Davison (2009)	Maintenance cost	2% of TCI (\$/a)
Ma et al. (2015)	Operating labor cost	0.8% of TCI (\$/a)
Ma et al. (2015)	Maintenance labor cost	0.8% of TCI (\$/a)
Ma et al. (2015)	Insurance	1% of TCI (\$/a)
Lee et al. (2021)	LH ₂	5.5 \$/kg

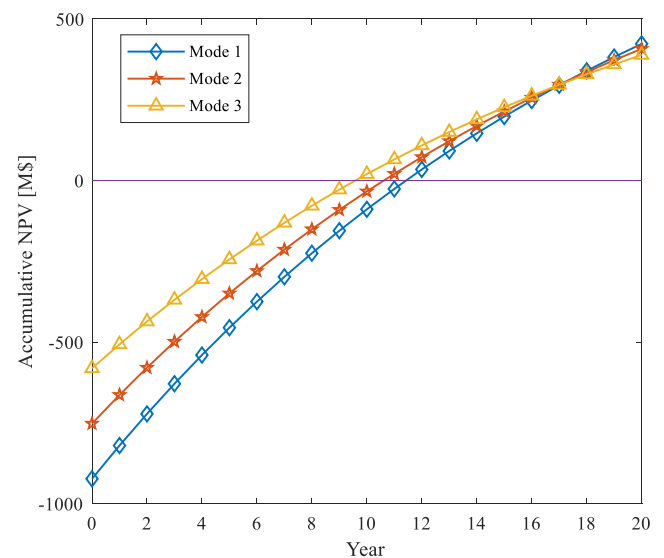


Fig. 18. Accumulative costs over the lifecycle of three modes.

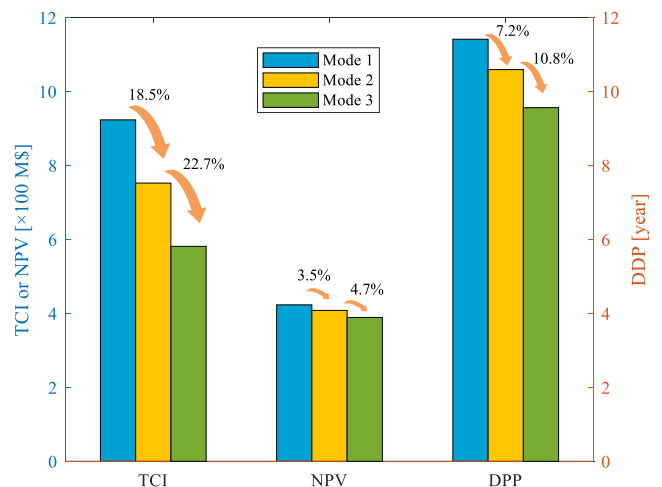


Fig. 19. Contrast of TCI, NPV and DPP with three modes.

mainly because when the price of the electrolytic cell drops, the price of the hydrogen tank has more impact on the initial investment of the system, and mode 1 does not require the use of hydrogen tanks.

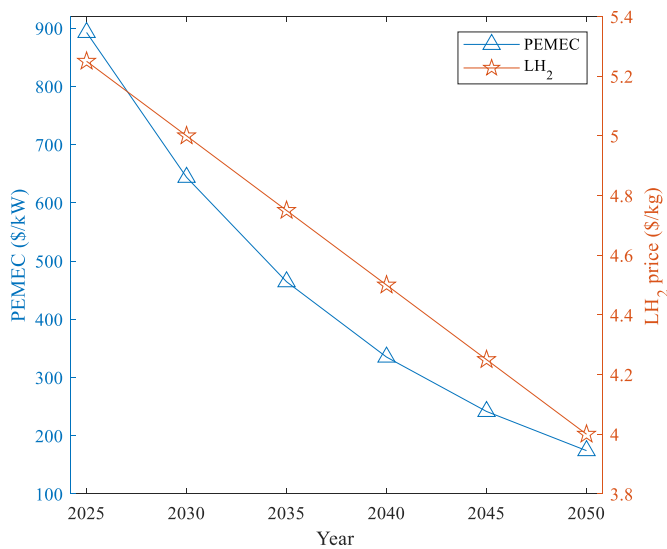


Fig. 20. Price prediction of electrolytic cell and liquid hydrogen.

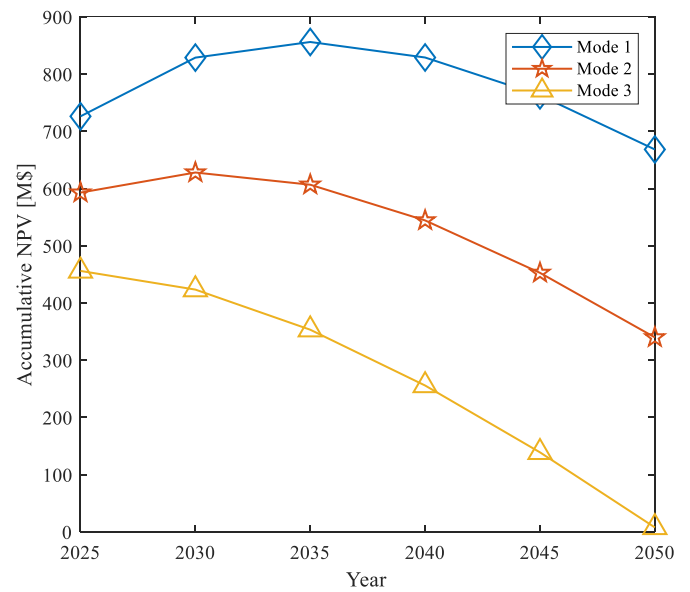


Fig. 22. Prediction of accumulative NPV over the lifecycle.

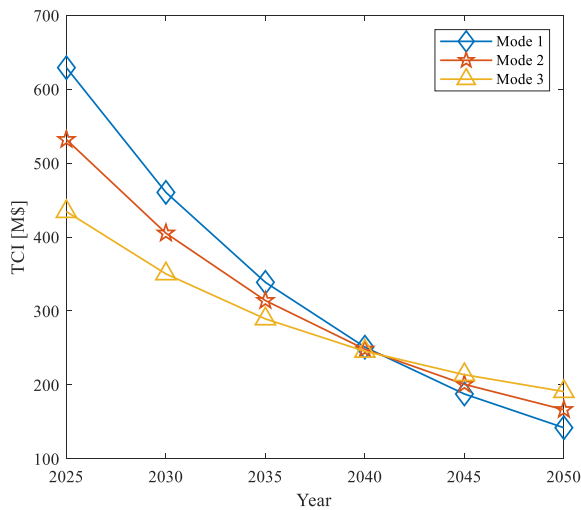


Fig. 21. Prediction of total capital investments.

As shown in Fig. 22, the net present value of mode 1 and mode 2 first increases and then decreases, while the net present value of mode 3 gradually decreases. Mode 1 reaches its maximum (856.2 M\$) in 2035, and mode 2 reaches its maximum (628.1 M\$) in 2030. Since 50% of the hydrogen in mode 3 comes from peak electricity, its operating cost is high. If the price of liquid hydrogen is low and this mode is still adopted, it will not be economical. Even if this mode is adopted in 2050, the cumulative net present value is only 7.9 M\$.

From Figs. 21 and 22, it can be found that in 2025, there is not much difference of the value (NPV-TCI) for all these 3 modes. When TCI increases, NPV cannot significantly increase. With the time going forward, the difference of NPV between the three modes will gradually increase, and the difference of TCI will also gradually decrease, and thus mode 2 and mode 3 will be more economical. In 2030, mode 2 and mode 3 are better than mode 1, and mode 2 can be chosen for higher NPV while mode 3 can be chosen for lower initial investment. In 2040, when the initial investment difference is not large, the NPV of mode 1 is much higher than that of mode 2 and mode 3. Therefore, from 2040, mode 1 will be more economically advantageous.

7. Conclusion

This paper proposes a novel scheme which uses surplus offshore wind power to produce hydrogen, and makes good use of LNG cold energy and liquid air technology to properly liquefy and store hydrogen. As a bridge between LNG and LH₂, liquid air can modify the fluctuation of natural gas load, and also provide stable cold energy for LH₂. Taking Hainan offshore wind power and Hainan LNG receiving station as the research objects, a new scheme of 100 MW hydrogen production and liquefaction has been designed, and the system process has been optimized and evaluated. Finally, the hydrogen gas is able to be liquefied with the optimal liquefaction process. In addition, considering three electrolytic hydrogen production modes, the economic feasibility of the new scheme is verified using dynamic economic modeling. The following conclusions can be drawn:

- (1) By optimizing the key node parameters of the system, the optimal pressure of LAES is 3 MPa and m_{LNG}/m_{air} is 0.32 in the 100 MW case study. The round-trip efficiency of liquid air is 71.0%, the exergy efficiency is 62.11%, and the specific energy consumption is 0.189 kWh/kg.
- (2) When the heat exchange temperature from liquid air is 86.95 K, the hydrogen liquefaction pressure is 8 MPa and the temperature is 31.15 K, the specific energy consumption of liquid hydrogen is the smallest. If the input hydrogen pressure is 0.1 MPa, the specific energy consumption of the liquid hydrogen is 7.87 kWh/kg, and the exergy efficiency of the whole system is 46.44%.
- (3) The economic analysis of three hydrogen production modes has been carried out. In 2025, it can be concluded that the mode 3 producing 50% hydrogen by peak electricity is more economical than that by valley electricity only (mode 1). In 2030, the mode 3 and the mode 2 producing 25% hydrogen by peak electricity will be more economical. In 2035, the mode 2 and mode 1 will be cheaper than mode 3. After 2040, the economic benefits of mode 1 will be the highest among three modes.

CRediT authorship contribution statement

Xiaoyuan Chen: Conceptualization, Methodology, Writing – original draft, Writing – review & editing, Supervision. **Jinxin Yue:** Investigation, Software, Visualization, Writing – original draft. **Lin Fu:** Investigation, Writing – review & editing, Supervision. **Mingshun**

Zhang: Methodology, Software. **Miangang Tang:** Software, Visualization. **Juan Feng:** Investigation, Visualization. **Boyang Shen:** Methodology, Writing – original draft, Writing – review & editing, Supervision.

Declaration of competing interest

The authors declare that they have no known competing financial interests or personal relationships that could have appeared to influence the work reported in this paper.

Data availability

Data will be made available on request.

Acknowledgements

This work was supported by the Sichuan Science and Technology Program [Grant No. 2023YFG0244 and No. 2022YFG0304] and National Natural Science Foundation of China [Grant No. 51807128].

References

- Abd Elbar, A.R., Yousef, M.S., Hassan, H., 2019. Energy, exergy, exergoeconomic and enviroeconomic (4E) evaluation of a new integration of solar still with photovoltaic panel. *J. Clean. Prod.* 233, 665–680.
- Akikur, R.K., Saidur, R., Ping, H.W., Ullah, K.R., 2014. Performance analysis of a co-generation system using solar energy and SOFC technology. *Energy Convers. Manag.* 79, 415–430.
- Ansarinasab, H., Fatimah, M., Khojasteh-Salkuyeh, Y., 2023. Performance improvement of air liquefaction processes for liquid air energy storage (LAES) using magnetic refrigeration system. *J. Energy Storage* 65, 107304.
- Asadnia, M., Mehroooya, M., 2017. A novel hydrogen liquefaction process configuration with combined mixed refrigerant systems. *Int. J. Hydrogen Energy* 42 (23), 15564–15585.
- Bae, J.E., Wilailak, S., Yang, J.H., Yun, D.Y., Zahid, U., Lee, C.J., 2021. Multi-objective optimization of hydrogen liquefaction process integrated with liquefied natural gas system. *Energy Convers. Manag.* 231, 113835.
- Battle, E.A.O., Palacio, J.C.E., Lora, E.E.S., Bortoni, E.D.C., Nogueira, L.A.H., Caballero, G.E.C., et al., 2021. Energy, economic, and environmental assessment of the integrated production of palm oil biodiesel and sugarcane ethanol. *J. Clean. Prod.* 311, 127638.
- Bian, J., Yang, J., Li, Y., Chen, Z., Liang, F., Cao, X., 2021. Thermodynamic and economic analysis of a novel hydrogen liquefaction process with LNG precooling and dual-pressure Brayton cycle. *Energy Convers. Manag.* 250, 114904.
- Bi, Y., Yin, L., He, T., Ju, Y., 2022. Optimization and analysis of a novel hydrogen liquefaction process for circulating hydrogen refrigeration. *Int. J. Hydrogen Energy* 47 (1), 348–364.
- Bi, Y., Ju, Y., 2022a. Conceptual design and optimization of a novel hydrogen liquefaction process based on helium expansion cycle integrating with mixed refrigerant pre-cooling. *Int. J. Hydrogen Energy* 47 (38), 16949–16963.
- Bi, Y., Ju, Y., 2022b. Design and analysis of an efficient hydrogen liquefaction process based on helium reverse Brayton cycle integrating with steam methane reforming and liquefied natural gas cold energy utilization. *Energy* 252, 124047.
- Central Government of the People's Republic of China, 2022. Hainan will build wind power 100 billion industrial cluster. http://www.gov.cn/xinwen/2022-07/17/content_5701420.htm. (Accessed 17 July 2022).
- Cerceanu, J., Mat, N., Junqua, G., Lin, L., Laforest, V., Gonzalez, C., 2014. Implementing industrial ecology in port cities: international overview of case studies and cross-case analysis. *J. Clean. Prod.* 74, 1–16.
- Chen, Q., Gu, Y., Tang, Z., Wang, D., Wu, Q., 2021a. Optimal design and techno-economic assessment of low-carbon hydrogen supply pathways for a refueling station located in Shanghai. *Energy* 237, 121584.
- Chen, X., Chen, Y., Zhang, M., Jiang, S., Gou, H., Pang, Z., Shen, B., 2021b. Hospital-oriented quad-generation (HOQG)—a combined cooling, heating, power and gas (CCHPG) system. *Appl. Energy* 300, 117382.
- Chen, X., Pang, Z., Jiang, S., Zhang, M., Peng, J., Fu, L., Shen, B., 2023a. A novel LH2/GH2/battery multi-energy vehicle supply station using 100% local wind energy: technical, economic and environmental perspectives. *Energy* 270, 126871.
- Chen, X., Pang, Z., Zhang, M., Jiang, S., Peng, J., Shen, B., 2023b. Techno-economic study of a 100-MW-class multi-energy vehicle charging/refueling station: using 100% renewable, liquid hydrogen, and superconductor technologies. *Energy Convers. Manag.* 276, 116463.
- Chen, X., Zhang, M., Jiang, S., Gou, H., Zhou, P., Yang, R., Shen, B., 2023c. Energy reliability enhancement of a data center/wind hybrid DC network using superconducting magnetic energy storage. *Energy* 263, 125622.
- Couper, J.R., Penney, W.R., James, R., Fair, P., 2009. *Chemical Process Equipment Revised 2E*. Elsevier Science.
- Davison, J., 2009. Criteria for Technical and Economic Assessment of Plants with Low CO₂ (sub 2) Emissions.
- Di Micco, S., Minutillo, M., Forcina, A., Cigolotti, V., Perna, A., 2021. Feasibility analysis of an innovative naval on-board power-train system with hydrogen-based PEMFC technology. In: *E3S Web of Conferences*, vol. 312. EDP Sciences, 07009.
- Dorosz, P., Wojcieszak, P., Malecha, Z., 2018. Exergetic analysis, optimization and comparison of LNG cold exergy recovery systems for transportation. *Entropy* 20 (1), 59.
- Energy Bureau of Shandong Province, 2023a. Construction machinery of the third phase of Qingdao LNG Receiving Station project has been completed. http://nyj.shandong.gov.cn/art/2023/7/31/art_253733_10299796.html. (Accessed 31 July 2023).
- Energy Bureau of Shandong Province, 2023b. During the 14th Five-Year Plan period, the output value of wind power industry chain will exceed 50 billion yuan. http://nyj.shandong.gov.cn/art/2023/3/29/art_253733_10296855.html. (Accessed 29 March 2023).
- Faramarzi, S., Nainiyan, S.M.M., Mafi, M., Ghasemiasl, R., 2021. A novel hydrogen liquefaction process based on LNG cold energy and mixed refrigerant cycle. *Int. J. Refrig.* 131, 263–274.
- Fusaro, R., Vercella, V., Ferretto, D., Viola, N., Steelant, J., 2020. Economic and environmental sustainability of liquid hydrogen fuel for hypersonic transportation systems. *CEAS Space Journal* 12, 441–462.
- Gao, Z., Ji, W., Guo, L., Fan, X., Wang, J., 2021. Thermo-economic analysis of the integrated bidirectional peak shaving system consisted by liquid air energy storage and combined cycle power plant. *Energy Convers. Manag.* 234, 113945.
- General administration of Customs, People's Republic of China. <http://www.customs.gov.cn/tjs/sjgb/4926700/4807029/index.html>. (Accessed 18 January 2023).
- Ghasemi, A., Heidarnajad, P., Noorpoor, A., 2018. A novel solar-biomass based multi-generation energy system including water desalination and liquefaction of natural gas system: Thermodynamic and thermoeconomic optimization. *J. Clean. Prod.* 196, 424–437.
- Ghorbani, B., Zendejboudi, S., Afrouzi, Z.A., 2023. Thermo-economic optimization of a novel hybrid structure for power generation and portable hydrogen and ammonia storage based on magnesium–chloride thermochemical process and liquefied natural gas cryogenic energy. *J. Clean. Prod.* 403, 136571.
- Gong, C., Li, L., Zhu, K., 2014. Agent-based simulations of time-of-use pricing of natural gas for resident customers. *J. Syst. Manag.* 23 (5), 682–689.
- Haacker, M., Hallett, T.B., Atun, R., 2020. On discount rates for economic evaluations in global health. *Health Pol. Plann.* 35 (1), 107–114.
- Jouybari, A.K., Ilinca, A., Ghorbani, B., Rooholamini, S., 2022. Thermodynamic and exergy evaluation of an innovative hydrogen liquefaction structure based on ejector-compression refrigeration unit, cascade multi-component refrigerant system, and Kalina power plant. *Int. J. Hydrogen Energy* 47 (62), 26369–26393.
- Khan, M.I., 2018. Evaluating the strategies of compressed natural gas industry using an integrated SWOT and MCDM approach. *J. Clean. Prod.* 172, 1035–1052.
- Kochunni, S.K., Chowdhury, K., 2020. Zero methane loss in reliquefaction of boil-off gas in liquefied natural gas carrier ships by using packed bed distillation in reverse Brayton system. *J. Clean. Prod.* 260, 121037.
- Lee, D., Gbadago, D.Q., Jo, Y., Hwang, G., Jo, Y., Smith, R., Hwang, S., 2021. Integrating hydrogen liquefaction with steam methane reforming and CO₂ liquefaction processes using techno-economic perspectives. *Energy Convers. Manag.* 245, 114620.
- Liu, X., Nguyen, M.Q., Chu, J., Lan, T., He, M., 2020. A novel waste heat recovery system combining steam Rankine cycle and organic Rankine cycle for marine engine. *J. Clean. Prod.* 265, 121502.
- Li, J., Zhang, Z., Zhang, S., Shi, F., Nie, Y., Xu, L., Ma, X., 2021. Life cycle assessment of liquefied natural gas production from coke oven gas in China. *J. Clean. Prod.* 329, 129609.
- Luo, Z., Hu, Y., Xu, H., Gao, D., Li, W., 2020. Cost-economic analysis of hydrogen for China's fuel cell transportation field. *Energies* 13 (24), 6522.
- Ma, L.C., Castro-Dominguez, B., Kazantzis, N.K., Ma, Y.H., 2015. Integration of membrane technology into hydrogen production plants with CO₂ capture: an economic performance assessment study. *Int. J. Greenh. Gas Control* 42, 424–438.
- Naquash, A., Qyyum, M.A., Islam, M., Sial, N.R., Min, S., Lee, S., Lee, M., 2022. Performance enhancement of hydrogen liquefaction process via absorption refrigeration and organic Rankine cycle-assisted liquid air energy system. *Energy Convers. Manag.* 254, 115200.
- National Energy Administration, 2012. The 3 million ton LNG project in Hainan is scheduled to start production in August 2014. http://www.nea.gov.cn/2012-07/11/c_131707587.htm. (Accessed 11 July 2012).
- National Energy Administration, 2023. Transcript of the second quarter of 2023 press conference of the National Energy Administration. http://www.nea.gov.cn/2023-04/27/c_1310714655.htm. (Accessed 27 April 2023).
- National Energy Communications Newsrooms, 2022. 12.3GW! Hainan offshore wind power "14th Five-Year Plan", released!. <http://gjnytx.com/zhengce/3177.html>. (Accessed 28 February 2022).
- Park, J., Qi, M., Kim, J., Noh, W., Lee, I., Moon, I., 2020. Exergoeconomic optimization of liquid air production by use of liquefied natural gas cold energy. *Energy* 207, 118193.
- Park, J., You, F., Mun, H., Lee, I., 2021. Liquefied natural gas supply chain using liquid air as a cold carrier: novel method for energy recovery. *Energy Convers. Manag.* 227, 113611.
- Peng, P., Lu, F., Cheng, S., Yang, Y., 2021. Mapping the global liquefied natural gas trade network: a perspective of maritime transportation. *J. Clean. Prod.* 283, 124640.
- Peng, X., She, X., Li, C., Luo, Y., Zhang, T., Li, Y., Ding, Y., 2019. Liquid air energy storage flexibly coupled with LNG regasification for improving air liquefaction. *Appl. Energy* 250, 1190–1201.
- People's Government of Guangdong Provincial, 2021. Notice of the general office of the Guangdong provincial People's government on issuing the implementation plan for

- promoting the orderly development of offshore wind power and the sustainable development of related industries. http://www.gd.gov.cn/zwgk/wjk/qbwj/yfb/content/post_3316639.html. (Accessed 11 June 2021).
- Qi, M., Park, J., Kim, J., Lee, I., Moon, I., 2020. Advanced integration of LNG regasification power plant with liquid air energy storage: enhancements in flexibility, safety, and power generation. *Appl. Energy* 269, 115049.
- Ratnakar, R.R., Gupta, N., Zhang, K., van Doorne, C., Fesmire, J., Dindoruk, B., Balakotiah, V., 2021. Hydrogen supply chain and challenges in large-scale LH2 storage and transportation. *Int. J. Hydrogen Energy* 46 (47), 24149–24168.
- Reddi, K., Elgowainy, A., Rustagi, N., Gupta, E., 2017. Impact of hydrogen refueling configurations and market parameters on the refueling cost of hydrogen. *Int. J. Hydrogen Energy* 42 (34), 21855–21865.
- Riaz, A., Qyyum, M.A., Hussain, A., Lee, M., 2022. Significance of ortho-para hydrogen conversion in the performance of hydrogen liquefaction process. *Int. J. Hydrogen Energy*.
- Riaz, A., Qyyum, M.A., Kim, G., Lee, M., 2021a. Harnessing liquid air cold energy for performance enhancement of hydrogen liquefaction process. In: *International Conference on Applied Energy*.
- Riaz, A., Qyyum, M.A., Min, S., Lee, M., 2021b. Performance improvement potential of harnessing LNG regasification for hydrogen liquefaction process: energy and exergy perspectives. *Appl. Energy* 301, 117471.
- Smith, R., 2005. *Chemical Process: Design and Integration*. John Wiley & Sons.
- State-owned Assets Supervision and Administration Commission of Guangdong Provincial People's Government, 2022. Guangdong Energy Group Huizhou LNG receiving Station project 150,000 ton berth supporting wharf construction started. http://gzww.gd.gov.cn/gkmlpt/content/4/4053/mmpost_4053690.html#1333. (Accessed 25 November 2022).
- Sung, T., Kim, K.C., 2017. LNG cold energy utilization technology. *Energy solutions to combat global warming* 47–66.
- Sun, Z., Lai, J., Wang, S., Wang, T., 2018. Thermodynamic optimization and comparative study of different ORC configurations utilizing the exergies of LNG and low grade heat of different temperatures. *Energy* 147, 688–700.
- Taghavi, M., Salarian, H., Ghorbani, B., 2021. Thermodynamic and exergy evaluation of a novel integrated hydrogen liquefaction structure using liquid air cold energy recovery, solid oxide fuel cell and photovoltaic panels. *J. Clean. Prod.* 320, 128821.
- The People's Government of Hainan Province, 2015. Suggestions on the utilization of LNG cold energy in Hainan and the national designated port for imported meat in Yangpu and the plan for the construction of frozen meat and other frozen product bases in Hainan. <https://www.hainan.gov.cn/rdjydata-5696.html> (Accessed 15 Octometer 2015).
- Wu, S., Zhou, C., Doroodchi, E., Moghtaderi, B., 2020. Techno-economic analysis of an integrated liquid air and thermochemical energy storage system. *Energy Convers. Manag.* 205, 112341.
- Xia, G., Sun, Q., Cao, X., Wang, J., Yu, Y., Wang, L., 2014. Thermodynamic analysis and optimization of a solar-powered transcritical CO₂ (carbon dioxide) power cycle for reverse osmosis desalination based on the recovery of cryogenic energy of LNG (liquefied natural gas). *Energy* 66, 643–653.
- Xie, C., Li, Y., Ding, Y., Radcliffe, J., 2019. Evaluating levelized cost of storage (lcos) based on price arbitrage operations: with liquid air energy storage (laes) as an example. *Energy Proc.* 158, 4852–4860.
- Xin, T., Xu, C., Li, R., Feng, Z., Yang, Y., 2022. An advanced coal-based zero-emission polygeneration system using water-gas shift reaction and syngas recycle to achieve different methanol and electricity distributions. *J. Clean. Prod.* 364, 132649.
- Xue, X., Guo, C., Du, X., Yang, L., Yang, Y., 2015. Thermodynamic analysis and optimization of a two-stage organic Rankine cycle for liquefied natural gas cryogenic exergy recovery. *Energy* 83, 778–787.
- Yang, J.H., Yoon, Y., Ryu, M., An, S.K., Shin, J., Lee, C.J., 2019. Integrated hydrogen liquefaction process with steam methane reforming by using liquefied natural gas cooling system. *Appl. Energy* 255, 113840.
- Yang, Y., Tong, L., Liu, Y., Guo, W., Wang, L., Qiu, Y., Ding, Y., 2023. A novel integrated system of hydrogen liquefaction process and liquid air energy storage (LAES): energy, exergy, and economic analysis. *Energy Convers. Manag.* 280, 116799.
- Yangjiang City natural resources Bureau high-tech distribution, 2023. Yangjiang municipal Bureau of natural resources high-tech branch on the "Yangjiang LNG peaking gas storage project export pipeline engineering use demonstration report" before the evaluation. http://www.yjgx.gov.cn/yjgxyjsgtzyjxqfj/gkmlpt/content/0/699/post_699015.html#4403. (Accessed 14 April 2023).
- Yin, L., Ju, Y., 2020. Process optimization and analysis of a novel hydrogen liquefaction cycle. *Int. J. Refrig.* 110, 219–230.
- Yue, J., Feng, J., Chen, J., Liu, R., Yu, C., Jiang, Z., et al., 2023. Multi-stage cold energy recovery/utilization: a 10 MW class cold store with liquefied natural gas. *Energy Sci. Eng.* 11 (2), 860–873.
- Yu, H., Yang, X., Chen, H., Lou, S., Lin, Y., 2022. Energy storage capacity planning method for improving offshore wind power consumption. *Sustainability* 14 (21), 14589.
- Zhang, G., Li, B., Zhang, X., Wang, Q., 2019. Design and simulation analysis of cold energy utilization system of LNG floating storage regasification unit. In: *IOP Conference Series: Earth and Environmental Science*, vol. 300. IOP Publishing, 022117, 2.
- Zhang, T., Chen, L., Zhang, X., Mei, S., Xue, X., Zhou, Y., 2018. Thermodynamic analysis of a novel hybrid liquid air energy storage system based on the utilization of LNG cold energy. *Energy* 155, 641–650.
- Zhang, T., Uratani, J., Huang, Y., Xu, L., Griffiths, S., Ding, Y., 2023. Hydrogen liquefaction and storage: recent progress and perspectives. *Renew. Sustain. Energy Rev.* 176, 113204.